On the Nature of Dynamical Instabilities in Interacting Binary Systems

Jacob Hooey

July 28, 2009

Bishop's University

A thesis submitted in partial fulfillment of the requirements for the degree of Bachelor of Science (Honours Physics)

Department of Physics

Bishop's University

Contents

Abstract

In this thesis we will analyze the limits of stability in interacting binaries containing compact accretors. . The specific case that will be used for this investigation is the case of Cataclysmic Variables (CVs) in which the donor star is still on (or close to) the Zero Age Main Sequence (ZAMS) at the onset of mass transfer to the white dwarf. Roche lobe geometry and angular momentum dissipation play an integral part in affecting the stability of the CV's evolution. The CV is said to be dynamically unstable when the rate of mass transfer from the donor to the accretor increases precipitously until it exceeds the Eddington Limit. At this point, the accretion luminosity becomes greater than the Eddington luminosity and the accretor (white dwarf) cannot accrete further mass. At this point the two stars share a common envelope and most likely combine into one larger mass (this is known as a merger). We comprehensively delineate the initial conditions (mass of the donor and mass of the accretor) for which binaries are stable and unstable. We also find, for the first time, dynamical runaways which occur long after the initial phase of mass transfer ($\Delta m \gtrsim 0.1 M_{\odot}$). We label this behavior as a "Latent Dynamical Instability" (LDI). The conditions for which LDIs occur have also been mapped out and are shown to be strongly correlated with the internal structure of the donor star.

Acknowledgments

I would like to express my gratitude to my thesis supervisor Dr. L. A. Nelson for his support and guidance throughout my academic career. His expertise and teaching methods were an integral part of my success at Bishop's University. I would also would like to thank Eric Blais, Julian Enright, and Jonas Goliasch for their assistance in the data collection and analysis phases of this thesis.

1 Introduction

1.1 Interacting Binary Systems

Cataclysmic Variables are systems of semi-detached binary stars containing a White Dwarf (WD) and a Zero Age Main Sequence (ZAMS) star (or possibly a more evolved star). These two stars are in such close proximity to each other that mass can be transferred from the ZAMS (donor) star onto the WD accretor (Hilditch 2001 [15]). An artist's conception of a CV can be seen in Figure 1. To classify of binary systems as semi-detached their Roche Lobe geometry must be determined. The critical Roche Lobe is a three-dimensional surface surrounding each individual star which is bounded by a common critical gravitational equipotential. When a star in the binary system expands beyond this envelope, the mass outside will be gravitationally attracted to the other star (through the inner Lagrange point) and therefore mass transfer begins. Other classifications include detached binary systems, where neither star fills its Roche Lobe and contact binaries which means that both stars share a common atmosphere and envelope. Contact binaries should not be confused with the common envelope stage of evolution which occurs as a result of dynamical instability. This dynamical instability can be caused by of the expansion of the massive donor star which results in a faster mass transfer rate to the point in which it is too fast to be accreted by the less massive companion star. At this point the frictional drag of the two envelopes causes the companion star to spiral in towards the core of the primary star and the conversion of orbital angular energy forces the common envelope to be ejected from the system. We will continue this introduction with a discussion of Roche Lobe Geometry.

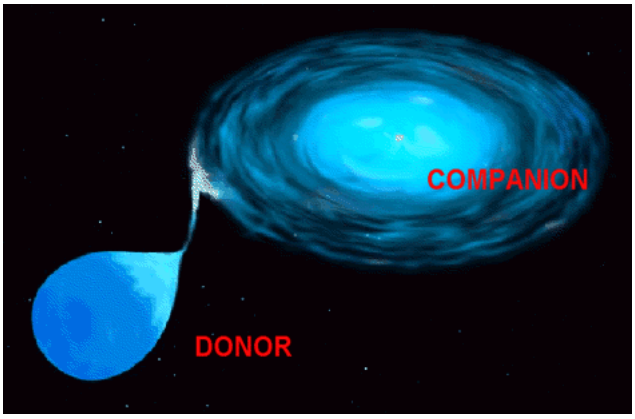

Figure 1: An artist's conception of a Cataclysmic Variable.

1.2 Roche Lobe Geometry

We will be using a non-inertial ($co-rotating$) Cartesian (x, y, z) reference frame, with the origin centered at the donor star. We define the x-axis to always be pointing towards the center of the WD, the y-axis to be in the plane of orbit and the z-axis is perpendicular to it. Using this coordinate system, the radius $r = \sqrt{x^2 + y^2 + z^2}$ defined in spherical coordinates, and a test particle of mass m, the gravitational and centripetal potential can be calculated for a test particle. This potential is given by Dubeau 2009 [1],

$$\Phi_G = -\frac{GM_1}{\sqrt{x^2+y^2+z^2}} - \frac{GM_2}{\sqrt{(x-A)^2+y^2+z^2}} - \frac{1}{2}G\left(\frac{m_T}{A^3}\right)\left[\left(x - \frac{M_1 A}{M_T}\right)^2 + y^2\right] \tag{1}$$

where A is the orbital separation, $M_T = M_1 + M_2$ is the total mass of the system, M_1 is the mass of the primary (WD) star and M_2 is the mass of the secondary (donor) star. By using the following unit-less variables,

$$\alpha = \frac{x}{A}, \beta = \frac{y}{A}, R_1' = \frac{\sqrt{(x-A)^2+y^2+z^2}}{A}, R_2' = \frac{\sqrt{x^2+y^2+z^2}}{A}, q = \frac{M_2}{M_1}$$

the formula simplifies to,

$$\Phi_G^{'} = \left(\frac{1}{1+q}\right)\left(\frac{1}{R_1^{'}} + \frac{q}{R_2^{'}}\right) + \frac{1}{2}\left[\left(\alpha - \frac{1}{1+q}\right)^2 + \beta^2\right]. \qquad (2)$$

The Roche Lobe ($R_L = f(M_2, M_T, A)$) is defined by the critical equipotential surface that intersects at the inner Lagrange point (L_1). The contour plot in Figure 2 shows the equipotential surfaces given by $\Phi_G^{'}$ and Figure 2 also shows a three-dimensional representation of the Roche Lobe passing through the inner Lagrange point.

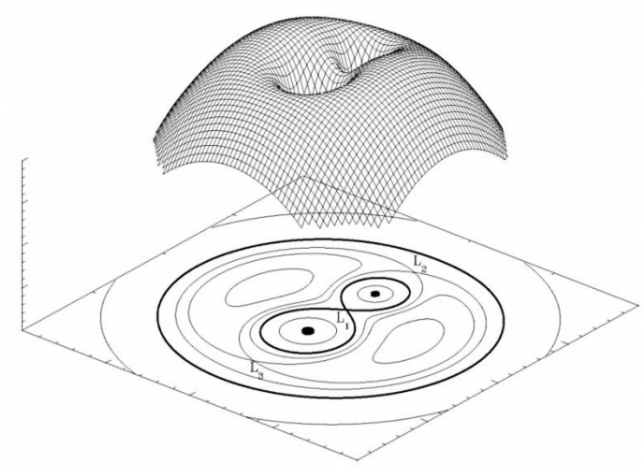

Figure 2: The Roche Lobe Equipotential Surface in Three-Dimensions with a Projected Contour Plot of all the Equipotential Surfaces given by $\Phi_G^{'}$.

If the radius (R_2) of the donor star is less than the volume-equivalent critical Roche lobe radius (R_L) then we consider this binary system to be detached with no mass transfer. On the other hand, if R_2 is slightly greater than R_L, then mass will be gravitationally pulled from the donor to the WD. The mass transfer rate can effectively change any of the following variables,M_1, M_2, M_T and R_2, which in turn can affect the mass transfer rate. Another factor that can affect the mass transfer rate is the rate of angular momentum dissipation from the binary system, which will be discussed in Section 1.3, the nuclear evolution of the donor (Dubeau 2009 [1]), and the response of the donor to mass loss (see, e.g., Rappaport et al. 1983 [2]) .

At a certain point, when all the mass outside of the donor's Roche lobe is being transferred to the WD, the radius of the Roche Lobe (R_L) approximately equates to the radius of the donor star (R_2), which we refer to as the effective Roche Lobe radius. The relation between the effective Roche lobe radius around the donor, $R_2 = R_L$, and the orbital separation, A, is only dependent on the mass ratio (Eggleton 1983 [3]), $q = \frac{M_2}{M_1}$, and is approximately given by,

$$R_2 = R_L \approx \frac{0.49q^{2/3}}{0.69q^{2/3} + ln(1 + q^{1/3})}A$$

Now if we were to take an even cruder approximation (D'Souza et al. 2005 [16]), which is correct within 6% for the range $0 < q < 4$, we get,

$$R_2 \approx 0.46\left(\frac{q}{1+q}\right)^{1/3} A = 0.46\left(\frac{M_2}{M_T}\right)^{1/3} A \tag{3}$$

1.3 Angular Momentum Dissipation

For the systems that we are considering, mass transfer will be driven by angular momentum losses. There are three prominent mechanisms for angular momentum loss: Gravitational Radiation, Magnetic Braking and Systemic Mass Loss.

1.3.1 Gravitational Radiation

If the quadrupole moment of the particles inside a system changes sufficiently quickly, there is an emission of gravitational waves, as predicted by Einstein's Theory of General Relativity. These waves carry energy and angular momentum from the system. When angular momentum is lost from the system, the orbital separation (A) of the two stars is decreased and therefore the orbital period also decreases. The energy carried out of the system is given by the Landau-Lifshitz formula (Rappaport et al. [2]):

$$\frac{dE}{dt} = -\frac{32}{5}\frac{G}{C^5}\omega^6 A^4 \left(\frac{M_1 M_2}{M_1 + M_2}\right)^2$$

Since the rate of change of the orbital angular momentum is directly related to the change in the energy, we can calculate the change in orbital angular momentum due to the loss of energy from gravitational radiation:

$$\frac{dJ}{dt} \equiv \dot{J}_{GR} = \frac{1}{\omega}\frac{dE}{dt} = -\frac{32}{5}\frac{G}{C^5}\omega^5 A^4 \left(\frac{M_1 M_2}{M_1 + M_2}\right)^2 \tag{4}$$

1.3.2 Magnetic Braking

Due to stellar winds, mass can stream out from the star along its magnetic field lines. The magnetic field lines then preserve the co-rotation of the ejected material out to a radius r_a, the Alfven radius. For a binary system in which the donor star is assumed to be tidally locked in a synchronized orbit, any loss of angular momentum in either star results in an angular momentum loss in the system. For magnetic braking, the generalized orbital angular momentum loss is given by the Verbunt-Zwaan law (Rappaport et al. 1983 [2])

$$\dot{J}_{MB} = -3.8 \times 10^{-30} M_2 R_\odot^4 \left(\frac{R_2}{R_\odot}\right)^\gamma \omega^3 \; dyne \cdot cm.$$

where γ is an arbitrary exponent in the range of 2 to 4.

1.3.3 Systemic Mass Loss

Angular momentum can also be advected from the binary due to mass loss from the system. To determine the momentum loss contribution due to mass loss we start with the equation for angular momentum,

$$\vec{J} = m(\vec{r} \times \vec{v})$$

and its magnitude for a circular orbit is

$$J = mvr$$

The change in angular momentum due to a change in the binary's mass is

$$\delta J = vr\delta m$$

where r is the distance from the center of mass and v is the (tangential) velocity. Considering now that $v = \omega r$ and that $\omega = \frac{2\pi}{P_{orb}}$, our δJ equation transforms into,

$$\frac{\delta J}{\delta m} = \frac{2\pi}{P_{orb}} r^2. \tag{5}$$

By determining the distances from each star to the center of mass, we get the two possible values of r:

$$r_1 = \left(\frac{M_2}{M_T}\right) A, \text{ and } r_2 = \left(\frac{M_1}{M_T}\right) A$$

where r_1 and r_2 are the orbital radii for the accretor and the donor, respectively. In our case, we are assuming that all the mass that is lost from the system originates on the accretion object. Therefore by substituting in the radius r_1 of the WD into equation (5) we get the angular momentum loss due to the mass lost from the accretor:

$$\left(\frac{\delta J}{\delta m}\right)_{accretor} = \frac{2\pi A^2}{P_{orb}} \left(\frac{M_2}{M_T}\right)^2. \tag{6}$$

Now consider the equation of the angular momentum of a binary system in circular orbit with each star treated as a point mass; that is,

$$J^2 = G\frac{M_1^2 M_2^2}{M_T} A$$

Combining it with the Kepler's Third Law relating orbital separation and angular velocity to the total mass,

$$\omega^2 A^3 = \left(\frac{2\pi}{P_{orb}}\right)^2 A^3 = GM_T$$

gives,

$$J = \frac{GM_1 M_2 P_{orb}}{2\pi A}.$$

Now by dividing both sides of equation (6) by J and further taking the limit of $\left(\frac{\delta J}{\delta m}\right)_{accretor}$ with respect to δt approaching zero, yields

$$\left(\frac{\dot{J}}{J}\right)_{MT} = \left(\frac{M_2}{M_T}\right)^2 \left(\frac{M_T}{M_1}\right) \left(\frac{\dot{M}_2}{M_2}\right)$$

which can also be written as,

$$\left(\frac{\dot{J}}{J}\right)_{MT} = \left(\frac{M_2}{M_1}\right) \left(\frac{\dot{M}_T}{M_T}\right) = q \left(\frac{\dot{M}_T}{M_T}\right) \tag{7}$$

This is the form of angular momentum dissipation due to systemic mass loss that will be used in all subsequent calculations.

1.4 Eddington Limit

For an ionized hydrogen particle (m_p) in a radiative and gravitational field, the Eddington Luminosity is defined such that the gravitational force inwards equals the radiative force outwards. In other words, this corresponds to the point when the accretion flow inwards would be completely choked off by the radiative pressure outwards. This definition assumes that the system is in hydrostatic quasi-equilibrium and has spherical symmetry. Now if we consider a WD that accretes mass at the rate $\dot{M}$ and that it converts all of that energy into radiation at its surface, then the accretion luminosity must be constrained to be less than the Eddington Luminosity (Soria 2003 [8]),

$$L_{acc} = \frac{GM_1\dot{M}_2}{R_1} < L_{edd} = \frac{4\pi GM_1 m_p c}{\sigma_T} = 1.3 \times 10^{38} \left(\frac{M_1}{M_\odot}\right) ergs/sec. \quad (8)$$

where R_1 is the radius of the accreting object, M_1 is the mass of the object, $\dot{M}_2$ is the mass transfer rate, σ_T is the Thomson cross-section of the electron, m_p is the mass of a proton falling onto the accretion object, c is the speed of light and $M_\odot$ is the mass of our sun.

In the case of a WD as the accretion object, the accretion luminosity is

$$L_{acc} = 1.3 \times 10^{33} \left(\frac{M_1}{M_\odot}\right) \left(\frac{\dot{M}_2}{1.5 \times 10^{-10} M_\odot yr^{-1}}\right) \left(\frac{R_1}{10^4 km}\right) ergs/sec.$$

In our case we will be using a WD of $1.4M_\odot$ as our limiting case, which has an approximate radius of $R = 10^3$km. Therefore the resultant Eddington Limit is approximately $\dot{M} = 1.5 \times 10^{-6} M_\odot yr^{-1}$. Throughout this thesis we will adopt the Eddington Limit to be approximately $1 \times 10^{-6} M_\odot yr^{-1}$.

When the accretion rate becomes greater than the Eddington Limit, the WD can no longer accrete all of the mass. This additional mass then begins to form a common envelope around the binary stars. The common envelope creates a frictional drag that causes the companion star to spiral in towards the core of the primary star. At this point the two stars are no longer distinguishable from each other and are therefore no longer considered to be part of a binary system. This leads to a merger.

1.5 The Type Ia Supernova Connection

We can ask the question as to why it matters whether a Cataclysmic Variable binary is stable or unstable. The answer is intimately connected to the observations of Type Ia Supernovae (Ia SNe). The recent discovery that the expansion of the universe is accelerating was a direct consequence of the observations of Ia SNe. Observations of the most distant of these supernovae showed them to be much fainter than expected (assuming that Ia SNe are good "standard candles"). Unfortunately the progenitors of Ia SNe are unknown. More than 40 years ago they were hypothesized to be Cataclysmic Variables for which the mass of the white dwarf accretor had been pushed beyond the Chandrasekhar Limit of 1.4 solar masses. Since the thermonuclear explosion that would result would always have the same amount of fuel (and hence brightness), it was thought that this mechanism would allow Ia SNe to be good standard candles.

It was soon realized that Classical Novae on the surface of the white dwarf accretor would expel as much mass during the thermonuclear runaway as was transferred over from the donor star (see DiStefano et al. 1195 [18]). Thus the mass of the white dwarf accretor could not grow and certainly could not grow beyond the Chandrasekhar Limit. However, about 10 years ago, Supersoft X-ray Sources (SSXSs) were discovered and it was quickly posited that the source of the X-rays was due to a steady nuclear burning on the surface of a white dwarf star. The reason that the burning was steady (as opposed to a Classical Novae runaway) was that the rate of mass transfer onto the surface of the white dwarf accretor was sufficiently high that thermonuclear runaways were suppressed. This can only happen for systems exhibiting very high rates of mass transfer on what is referred to as a Kelvin-Helmholtz or thermal timescale.

If the mass transfer rate becomes too high, as in the case of dynamical instability, then the binary system components merge into a single object and a Ia SNe is not possible. Thus it is absolutely critical when doing population synthesis studies (i.e. to determine the expected frequency Ia SNe assuming that their progenitors are interacting binaries) to know the initial conditions separating Kelvin-Helmholtz mass transfer from dynamically unstable mass transfer (see DiStefano et al. 1195 [18]). One of the surprises discovered in this work is that Latent Dynamical Instabilities allow large amounts of mass to be transferred onto the white dwarf (where steady burning conditions obtain), before dynamical instability prevents further growth in the mass

of a white dwarf (see Section 3.3.4 for more details). Thus it is possible for many more white dwarfs than had previously been expected to grow in mass in excess of the Chandrasekhar Limit and thereby undergo a Type Ia Supernova explosion.

2 Stability Condition

2.1 Calculating the Stability Condition Analytically

The orbital angular momentum of a binary system in circular orbit with each star treated as a point mass is given by

$$J^2 = G\frac{M_1^2 M_2^2}{M_T}A \tag{9}$$

where J is the orbital angular momentum, G is the gravitational constant, M_1 is the mass of the accreting star, M_2 is the mass of the donor star , M_T is the total mass of the donor and accreting stars and A is the orbital separation.

We want to study the temporal behavior of the binary system and therefore we will need to include the rate of change in angular momentum. By taking the derivative of equation (9) we obtain:

$$2\frac{\dot{J}}{J} = 2\frac{\dot{M_1}}{M_1} + 2\frac{\dot{M_2}}{M_2} + \frac{\dot{A}}{A} - \frac{\dot{M_T}}{M_T} \tag{10}$$

We will also need to incorporate the rate of change in the orbital separation over time which is found by taking the derivative of equation (3) which was discussed in Section 1.2. Thus

$$\frac{\dot{A}}{A} \cong \frac{\dot{R_2}}{R_2} - \frac{1}{3}\frac{\dot{M_2}}{M_2} + \frac{1}{3}\frac{\dot{M_T}}{M_T} \tag{11}$$

Now if we substitute equation (11) into equation (10) we get,

$$2\frac{\dot{J}}{J} = 2\frac{\dot{M_1}}{M_1} + \frac{5}{3}\frac{\dot{M_2}}{M_2} - \frac{2}{3}\frac{\dot{M_T}}{M_T} + \frac{\dot{R_2}}{R_2} \tag{12}$$

which no longer explicitly depends on the orbital separation or the rate of change of the orbital separation.

Now we define a new variable $\beta = -\frac{\dot{M_1}}{\dot{M_2}}$, which describes the ratio between the changes of mass in each star. If this value is equal to 1, this means that all the mass lost from the donor is gained by the other one and therefore we have mass conservation. However, if this ratio is not 1, then we have mass that is being taken out of our binary system; therefore mass is not conserved.

We can now look at each individual component of equation (12) and redefine them in terms of β.

$$\dot{M}_T = \dot{M}_1 + \dot{M}_2 = \dot{M}_2 \left(1 - \beta\right),$$

$$\frac{\dot{M}_1}{M_1} = -\frac{\dot{M}_2}{M_1}\left(-\frac{\dot{M}_1}{\dot{M}_2}\right) = -\frac{\dot{M}_2}{M_1}\beta = \frac{-\dot{M}_2}{M_2}\left(\frac{M_2}{M_1}\right)\beta,$$

and

$$\frac{\dot{M}_T}{M_T} = \frac{\dot{M}_2\left(1-\beta\right)}{M_T} = \frac{2\dot{M}_2}{M_2}\left(\frac{M_2}{2M_T}\right)\left(1-\beta\right)$$

Now we consider the implications of $\frac{\dot{R}_2}{R_2}$ in equation (12). It is convenient to express the radius in terms of the mass as $R_2 = M_2^{\xi}$ where ξ is the stellar index. Now if we take the time derivative of this relation we get,

$$\frac{\dot{R}_2}{R_2} = \xi\frac{\dot{M}_2}{M_2}.$$

In some ways, ξ can be thought of as a measure of the donor star's response to mass loss. In fact if the star is fully convective (i.e. $M_2 \lesssim 0.35M_{\odot}$), it can be shown that $\xi \cong \xi_{adiabatic} = -\frac{1}{3}$ (Rappaport et al. 2001 [6], and King and Kolb 1999 [7]). Thus convective stars that lose mass $\left(\dot{M}_2 < 0\right)$ will expand (i.e. $\dot{R}_2 > 0$). For solar-type stars, ξ is typically of order unity and these stars thus tend to shrink due to mass loss. Inserting the four equations above into equation (12) we get,

$$\frac{\dot{J}}{J} = \frac{\dot{M}_2}{M_2}\left[\frac{5}{6} + \left(-\frac{M_2}{M_1}\right)\beta - \left(\frac{M_2}{3M_T}\right)\left(1-\beta\right) + \frac{\xi}{2}\right] \tag{13}$$

Now, the total change of angular momentum of the system over time $(\dot{J})$ is simply the sum of the amount of angular momentum carried away by gravitational radiation, magnetic braking, and mass lost from the system (see section 1.3.3). The angular momentum lost through gravitational radiation and magnetic braking can be expressed as $\dot{J}_{AML}$ and systemic losses can be written as $\left(\frac{\dot{J}}{J}\right)_{MT} = \left(\frac{\dot{M}_T}{M_T}\right) f(M_1, M_2, \beta)$. Therefore, $\frac{\dot{J}}{J}$ can also be described as follows:

$$\frac{\dot{J}}{J} = \left(\frac{\dot{J}}{J}\right)_{AML} + \left(\frac{\dot{J}}{J}\right)_{MT} = \left(\frac{\dot{J}}{J}\right)_{AML} + \left(\frac{\dot{M}_T}{M_T}\right) f(M_1, M_2, \beta) \tag{14}$$

If we equate equation (13) and equation (14), we get

$$\left(\frac{\dot{J}}{J}\right)_{AML} + \left(\frac{\dot{M}_T}{M_T}\right) f(M_1, M_2, \beta) = \frac{\dot{M}_2}{M_2}\left[\frac{5}{6} + \left(-\frac{M_2}{M_1}\right)\beta - \left(\frac{M_2}{3M_T}\right)(1-\beta) + \frac{\xi}{2}\right]$$

Now solving for $\dot{M}_2/\ M_2$ yields

$$\frac{\dot{M}_2}{M_2} = \frac{\left(\frac{\dot{J}}{J}\right)_{AML}}{\left[\frac{5}{6} + \left(-\frac{M_2}{M_1}\right)\beta - \left(f + \frac{1}{3}\right)\left(\frac{M_2}{M_T}\right)(1-\beta) + \frac{\xi}{2}\right]}$$

Substituting in $q = \frac{M_2}{M_1}$ gives

$$\frac{\dot{M}_2}{M_2} = \frac{\left(\frac{\dot{J}}{J}\right)_{AML}}{\left[\frac{5}{6} - q\beta - \left(f + \frac{1}{3}\right)\left(\frac{q}{1+q}\right)(1-\beta) + \frac{\xi}{2}\right]} \tag{15}$$

In this analysis we will consider the system unstable once its mass transfer rate exceeds the approximate Eddington Limit (Section 1.4). We can see that the mass transfer rate described in equation (15) becomes extremely large when the denominator tends to zero. Therefore we know that the mass transfer rate exceeds the Eddington Limit when the denominator equals zero. This is formally the definition of dynamical instability.

Thus the condition leading to instability can be written as

$$\left[\frac{5}{6} - q_{cr}\beta - \left(f + \frac{1}{3}\right)\left(\frac{q_{cr}}{1+q_{cr}}\right)(1-\beta) + \frac{\xi}{2}\right] = 0 \tag{16}$$

Note that q_{cr} is the critical value of q for which this condition holds.

2.1.1 Conservative Mass Transfer ($\beta = 1$)

Consider the special case where no mass is lost from the system; hence we will use $\beta = 1$. Equation (16) becomes

$$q_{cr} = \frac{5}{6} + \frac{\xi}{2}$$

Now if we consider an adiabatic index of $\xi = -1/3$ for a low-mass (convective) star, we get a value of

$$q_{cr} = \frac{M_2}{M_1} = \frac{2}{3}$$

From this result we can say that the mass of the donor must be less than two-thirds the mass of the accreting star for this system to be stable. If the the value of q is greater than $2/3$, the donor star expands more rapidly than the Roche lobe. Therefore, if the donor star is initially more massive than the accretor, the orbital separation will decrease with time and the effective radius of the Roche lobe will decrease as well. Since the donor can expand due to mass loss (Tout et al. 1997 [11]), mass transfer will be clearly unstable for this case.

2.1.2 Fully Non-Conservative Mass Transfer ($\beta = 0$)

This case is also the case that will be investigated numerically in this thesis (it is a more physically realistic model for CVs undergoing classical nova explosions). In this case all the mass accreted by the WD will be lost out of the system through nova explosions. Therefore if $\beta = 0$, equation (16) becomes,

$$\left[\frac{5}{6} - \left(f + \frac{1}{3}\right)\left(\frac{q_{cr}}{1+q_{cr}}\right) + \frac{\xi}{2}\right] = 0$$

$$q_{cr} = \frac{3\xi + 5}{6f - 3}. \tag{17}$$

Now if we consider the momentum lost from the system due to the mass lost from the binary we can use equation (5) from Section 1.3.3,

$$\left(\frac{\dot{J}}{J}\right)_{MT} = q\left(\frac{\dot{M}_T}{M_T}\right).$$

If we compare this to the systemic mass loss component of equation (14), $\left(\frac{\dot{J}}{J}\right)_{MT} = \left(\frac{\dot{M}_T}{M_T}\right) f(M_1, M_2, \beta)$, we get,

$$f(M_1, M_2) = q$$

Substitute this value into equation (17) and choosing the adiabatic index for a low-mass (convective) star ($\xi = -1/3$) , we get, $3q_{cr}^2 - q_{cr} - 2 = 0$, which results in a q_{cr} value of

$$q_{cr} = 1 \tag{18}$$

These results are not in contradiction with previous analysis such as those by Soberman et al. (1997 [4]) and Hjellming and Webbink (1987 [5]).

3 Stellar Model Calculations

Because the value of ξ is inextricably linked to the response of the donor star to mass loss, its nuclear evolution, and its mass-loss history, it cannot be calculated analytically in a completely general way. Thus a numerical approach must be taken wherein a detailed physical model of the donor star is computed allowing for the temporal evolution to be calculated.

3.1 Henyey Method

The Henyey method treats stellar evolution as a simple initial value problem which is only dependent on time t and a complex boundary value problem which is dependent only on M_r. Any other of the other (dependent) variables (i.e. P, T, r, L) can be written as functions of these two (independent) variables. The extrapolation in time is treated using a simple explicit linear method while the spatial part of the problem is treated using difference equations and a relaxation technique to solve for these equations (Dubeau 2009 [1]).

A trial solution is found for each difference equation for a fixed interval of time (Δt). Every consecutive iteration afterwards improves these solutions. To minimize the error on the interval's overall solution, corrections are made to each variable until the desired accuracy is reached. The stellar evolution is therefore determined by the rate of mass loss, a set of coupled differential equations, restricted by boundary conditions at the surface and center of the donor star. To simplify the calculations, the Henyey method makes several assumptions. Due to the fact that it is using only two independent variables t and M_r, with all other variables being dependent, the assumptions that are described by Dubeau (2009 [1]) are as follows:

1. The star is spherically symmetric. This implies that the method excludes magnetic forces, tidal forces and stellar rotation.

2. Density, pressure and chemical composition are time independent. Therefore they only depend on the mass interior to the shell (M_r). This implies that elements in a given mass shell have a homogeneous composition.

3. The mass of the system remains constant during a given timestep (Δt). The mass is removed at the beginning of the following model.

4. Inefficient convection (convection combined with radiative transport) is included only when the envelope is being calculated. Simple mixing length theory is used to describe the adiabatic convection.

With the above assumptions, the functional description of a star can be written as

$$f\left(P\left(M_r,t\right),T\left(M_r,t\right),r\left(M_r,t\right),L_r\left(M_r,t\right),X_i\left(M_r,t\right)\right) \tag{19}$$

In summary, the Henyey method is a numerical relaxation scheme used to solve differential equations wherein the boundary conditions are given at each end of the boundary. A full and in-depth analysis of the Henyey method is given by Dubeau (2009 [1]).

3.2 Input Parameters

There are only two input parameters that we use to investigate the stability of the binary system. These parameters are the mass of the WD (M_1) and the mass of the donor star (M_2). These two parameters are restricted due to the Chandrasekhar limit for the WD mass ($M_1 \leq 1.4M_\odot$) and the limits of the outer boundary value condition table ($M_2 \leq 2.2M_\odot$) required by the Henyey method. The chemical profile is another input parameter that could be changed (to account for nuclear evolution), but this is beyond the scope of this thesis (see section 4.1 for a discussion). Thus all of our models begin Roche Lobe overflow when they are still on the Zero-Age Main Sequence.

3.2.1 The Chandrasekhar Limit

For a body consisting of electron-degenerate matter, its total mass is limited by the Chandrasekhar limit. This limit is the maximum non-rotating mass which can be supported against gravitational collapse by electron degeneracy pressure. Seeing as WDs consist entirely of electron-degenerate matter, they are bounded by the Chandrasekhar limit, which is calculated to be approximately $1.4M_\odot$ for an appropriate mixture of Carbon and Oxygen.

3.3 Mass-Loss Regimes

Until recently there have been three mass loss regimes that have been widely accepted and studied by the astrophysical community. Stable mass transfer,

thermal timescale mass transfer, and dynamical instability have been well documented (Rappaport et al. (1983) [2], Rappaport et al. (1982) [9], Han et al. (2002) [10], King et al. (2001) [12], Ivanova et al. (2004) [13] and de Kool (1992) [14]). But there is also the very interesting case of latent dynamical instability that was discovered to be quite common in the higher WD and donor-mass region.

3.3.1 Stable Mass Transfer

Stable mass transfer is the classic example of CV evolution. It is the case where the donor transfers mass steadily thoughout its evolution. Figure 3 is a good example of a stable CV evolution.

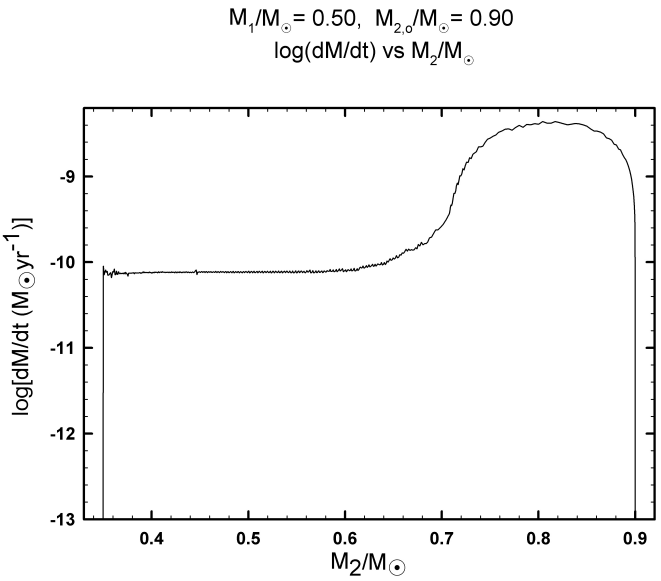

Figure 3: Mass loss rate $\log\left[\frac{dM}{dt}\left(M_{\odot}yr^{-1}\right)\right]$ vs. Donor Mass $\left(\frac{M_2}{M_{\odot}}\right)$ - An Example of a Stable CV track, with a constant WD mass (M_1).

3.3.2 Thermal Timescale Mass Transfer

Thermal Timescale Mass Transfer (TTMT) is a stable case of CV evolution. The difference between TTMT and normal stability is a long period during the evolution in which there is a very high mass transfer rate $\left(10^{-8} \lesssim \left|\dot{M}_2/\left(M_{\odot}yr^{-1}\right)\right| \lesssim 10^{-6}\right)$. The time during which a system exhibits

a very high rate of mass transfer is referred to as a Kelvin-Helmholtz or thermal timescale. Figure 4 depicts a good example of extended TTMT.

This can only happen for systems exhibiting very high rates of mass transfer on what is referred to as a Kelvin-Helmholtz or thermal timescale. This type of behavior is common in systems where the mass of the donor is moderately high and the initial mass ratio (q_o) exceeds ≈ 1.5.

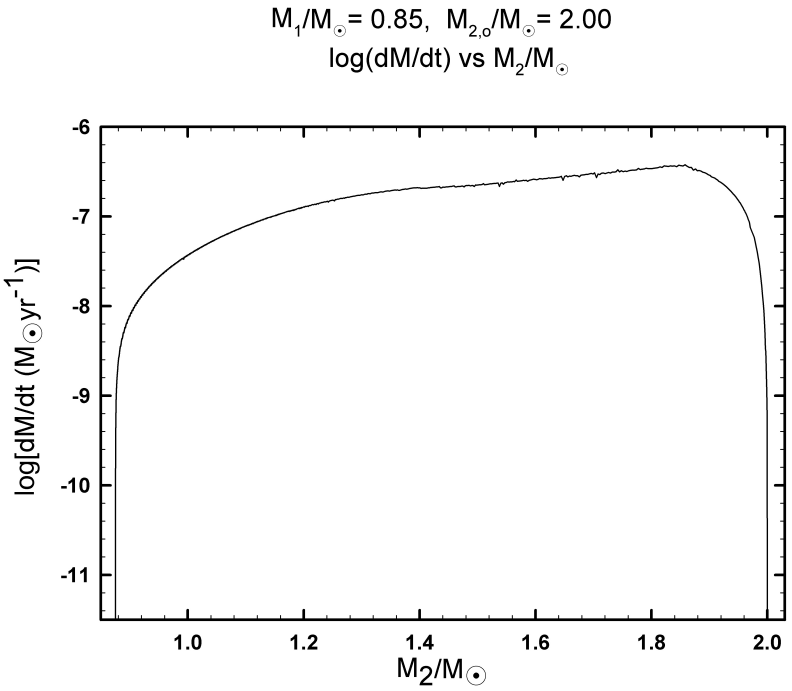

Figure 4: Mass loss rate $\log\left[\frac{dM}{dt}\,(M_{\odot}yr^{-1})\right]$ vs. Donor Mass $\left(\frac{M_2}{M_{\odot}}\right)$ - An Example of a Thermal Timescale Mass Transfer CV track, with a constant WD mass (M_1).

3.3.3 Dynamical Instability

Dynamical instability (DI) is defined by the fact that quite early on in the CVs evolution, the mass transfer rate increases rapidly and reaches the Eddington Limit. Figure 5 is an example of a dynamically unstable CV. As the plot shows, the system reaches the Eddington limit before the donor was able to lose more than $0.01M_{\odot}$ of its mass. For these cases, it makes almost no difference whether the binary system loses orbital angular momentum by

either gravitational radiation or magnetic braking.

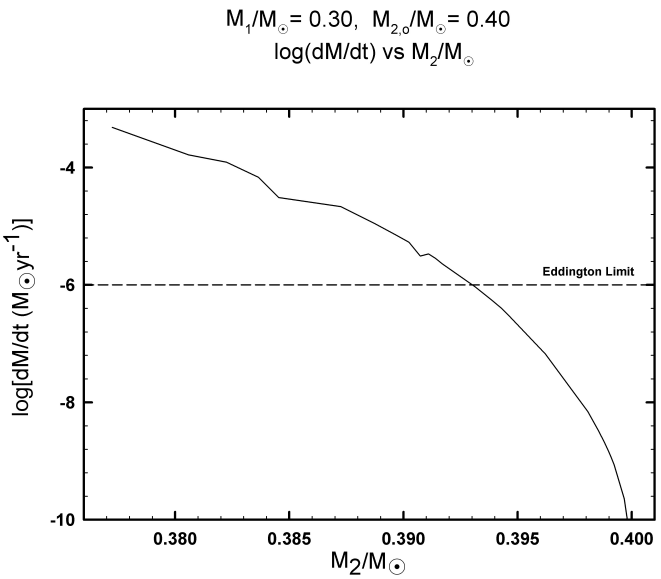

Figure 5: Mass loss rate $\log\left[\frac{dM}{dt}\left(M_{\odot}yr^{-1}\right)\right]$ vs. Donor Mass $\left(\frac{M_2}{M_{\odot}}\right)$ - An Example of a Dynamically Unstable CV track, with a constant WD mass (M_1).

3.3.4 Latent Dynamical Instability

Latent Dynamical instability (LDI) is very similar to DI in the respect that the evolution finishes with mass transfer rates exceeding the Eddington Limit. Figure 6 is an example of a dynamically unstable CV. As the plot shows, the system reaches the Eddington limit after a long steady thermal timescale of mass loss before the donor was pushed past the Eddington limit. This is greatly due to the way that the donor's thermal structure reacts to mass loss. At a certain point, as the donor loses mass, the fraction of the star (by mass) that contains the convective zone gets larger than that for the radiative zone. Recall that ξ can be negative for convective stars (and positive for radiative ones). As can be seen in equation (15), the denominator is a function of ξ. As ξ diminishes the denominator gets smaller and this leads to an increase in $\left|\dot{M}_2\right|$. This is the qualitative description for the behavior of LDIs.

It is interesting to note that the condition leading to instability (see equation (16)) depends on both ξ and q. As CVs evolve, their value of q must

decrease which almost always implies greater stability. However, the effective value of ξ changes and for the LDI cases, the effects of a decreasing ξ (i.e., towards greater instability), swamp out the effects of a decreasing value of q (i.e., towards greater stability) thus leading to a "late instability". Another example of an LDI is shown in 7

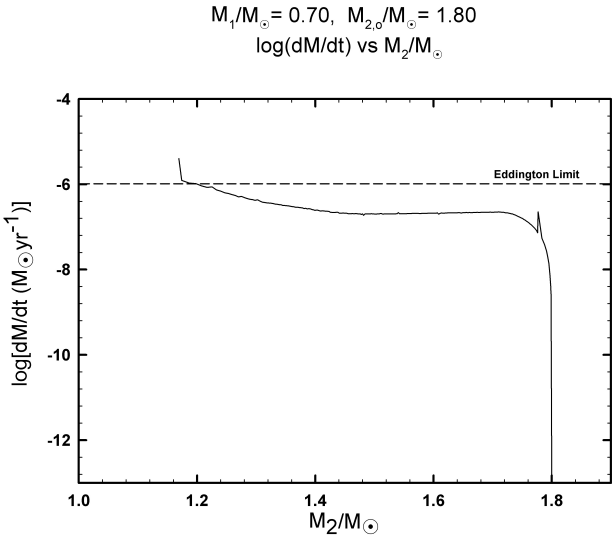

Figure 6: Mass loss rate $\log\left[\frac{dM}{dt}\left(M_{\odot}yr^{-1}\right)\right]$ vs. Donor Mass $\left(\frac{M_2}{M_{\odot}}\right)$ - An Example of a Latent Dynamically Unstable CV track, with a constant WD mass (M_1).

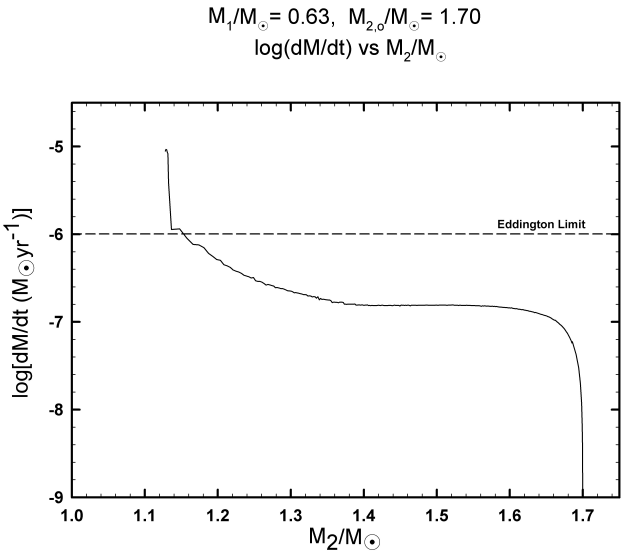

Figure 7: Mass loss rate $\log\left[\frac{dM}{dt}\,(M_{\odot}yr^{-1})\right]$ vs. Donor Mass $\left(\frac{M_2}{M_{\odot}}\right)$ - Another Example of a latent dynamically unstable CV track, with a constant WD mass (M_1).

3.4 Results

Ninety three cases of CV evolution were run on the Mammouth Serial 2 and Nelson-ms supercomputers to try to determine the boundary between stability and instability. Only a limited number of donor models were available, but $\left(\frac{M_1}{M_{\odot}}\right)$ were chosen to be at intervals as small as $0.01M_{\odot}$. Figure 8 displays all of the tracks that were calculated, and labels them according to their stability category.

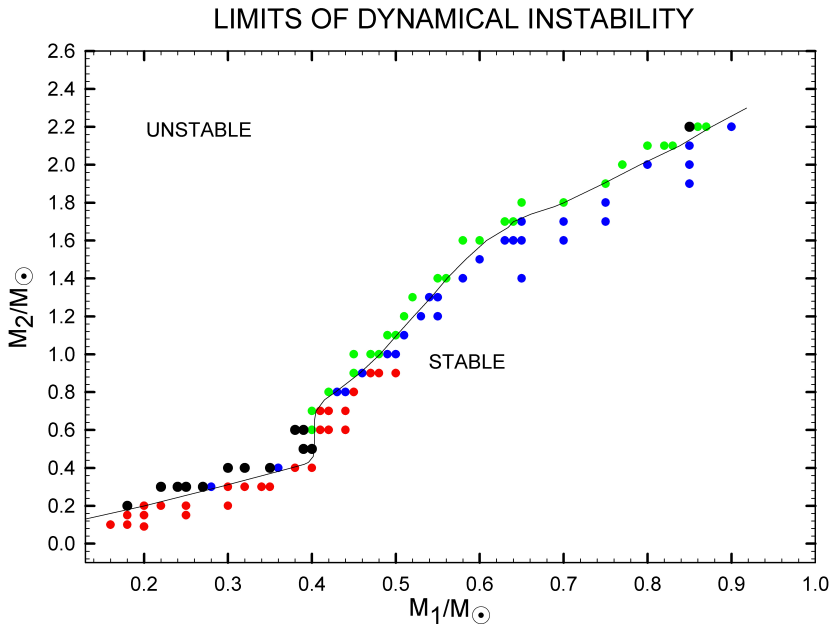

Figure 8: $\left(\frac{M_2}{M_\odot}\right)$ vs. $\left(\frac{M_1}{M_\odot}\right)$ - Summary of all the CV tracks that were computed. Red points depict tracks that were in the range of normal stability, blue points shows tracks that experienced thermal timescale mass transfer, black points are tracks that were truly dynamically unstable while the green points are tracks that experienced latent dynamical instability.

3.4.1 Representative Data

Each point in Figure 8 represents a CV evolution. The following figures are a representative sample of sets of two values for each WD mass that show the upper and lower constraints of stability. On each of the following pages there will be two CV evolution tracks for the same WD mass $\left(\frac{M_1}{M_\odot}\right)$ but different donor masses $\left(\frac{M_2}{M_\odot}\right)$. Each donor mass will be separated by only a single interval ($0.1M_\odot$ for almost all cases) of the available masses. The first plot of the set of two corresponds to a stable CV evolution while the second is unstable. This demonstrates how the upper and lower bounds of stability were clearly distinguished.

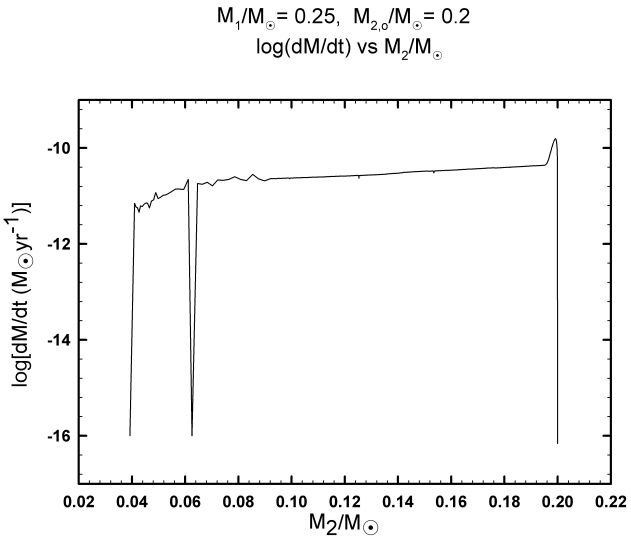

Figure 9: $\log\left[\frac{dM}{dt}\,(M_{\odot}yr^{-1})\right]$ vs. Donor Mass $\left(\frac{M_2}{M_{\odot}}\right)$ - Stable CV with starting masses $\left(\frac{M_1}{M_{\odot}}\right) = 0.25$ and $\left(\frac{M_2}{M_{\odot}}\right) = 0.2$

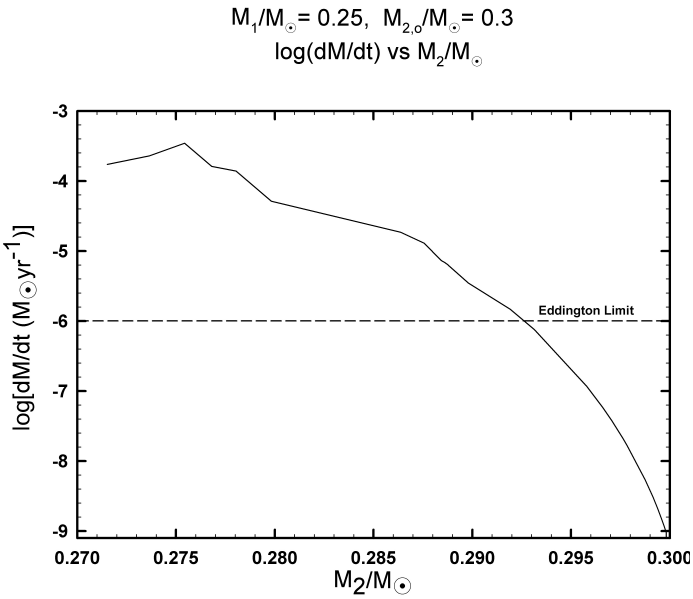

Figure 10: $\log\left[\frac{dM}{dt}\left(M_{\odot}yr^{-1}\right)\right]$vs. Donor Mass $\left(\frac{M_2}{M_{\odot}}\right)$ - Dynamically Unstable CV with starting masses $\left(\frac{M_1}{M_{\odot}}\right) = 0.25$ and $\left(\frac{M_2}{M_{\odot}}\right) = 0.30$

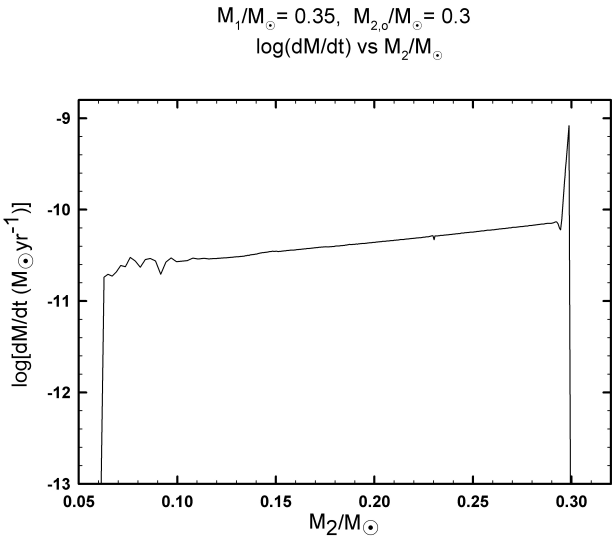

Figure 11: $\log\left[\frac{dM}{dt}\left(M_{\odot}yr^{-1}\right)\right]$ vs. Donor Mass $\left(\frac{M_2}{M_{\odot}}\right)$ - Stable CV with starting masses $\left(\frac{M_1}{M_{\odot}}\right) = 0.35$ and $\left(\frac{M_2}{M_{\odot}}\right) = 0.30$

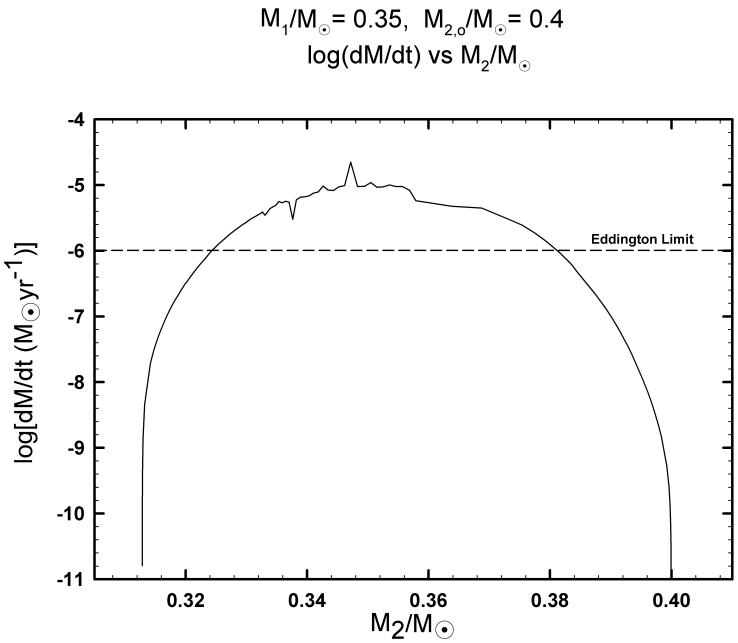

Figure 12: $\log\left[\frac{dM}{dt}\,(M_{\odot}yr^{-1})\right]$vs. Donor Mass $\left(\frac{M_2}{M_{\odot}}\right)$ - Dynamically Unstable CV with starting masses $\left(\frac{M_1}{M_{\odot}}\right) = 0.35$ and $\left(\frac{M_2}{M_{\odot}}\right) = 0.40$

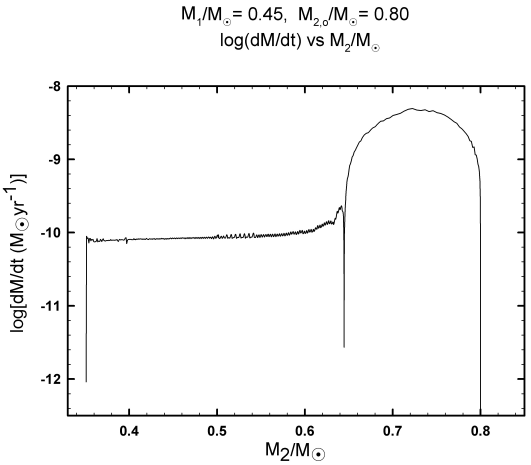

Figure 13: $\log\left[\frac{dM}{dt}\left(M_{\odot}yr^{-1}\right)\right]$vs. Donor Mass $\left(\frac{M_2}{M_{\odot}}\right)$ - Stable CV with starting masses $\left(\frac{M_1}{M_{\odot}}\right) = 0.45$ and $\left(\frac{M_2}{M_{\odot}}\right) = 0.80$

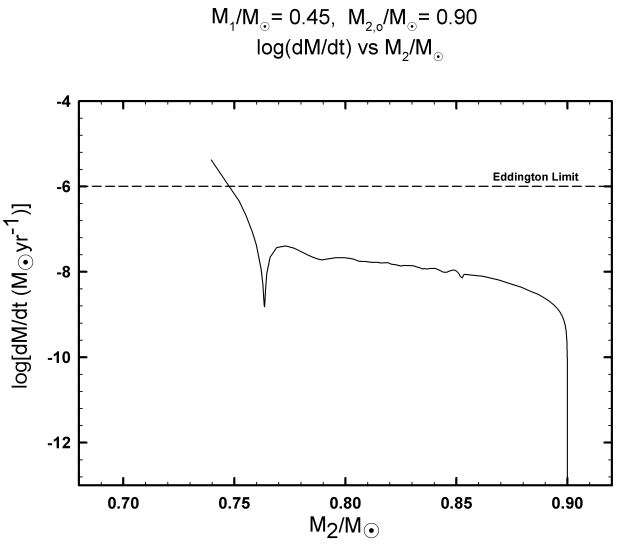

Figure 14: $\log\left[\frac{dM}{dt}\left(M_{\odot}yr^{-1}\right)\right]$vs. Donor Mass $\left(\frac{M_2}{M_{\odot}}\right)$ - Latent Dynamically Unstable CV with starting masses $\left(\frac{M_1}{M_{\odot}}\right) = 0.45$ and $\left(\frac{M_2}{M_{\odot}}\right) = 0.90$

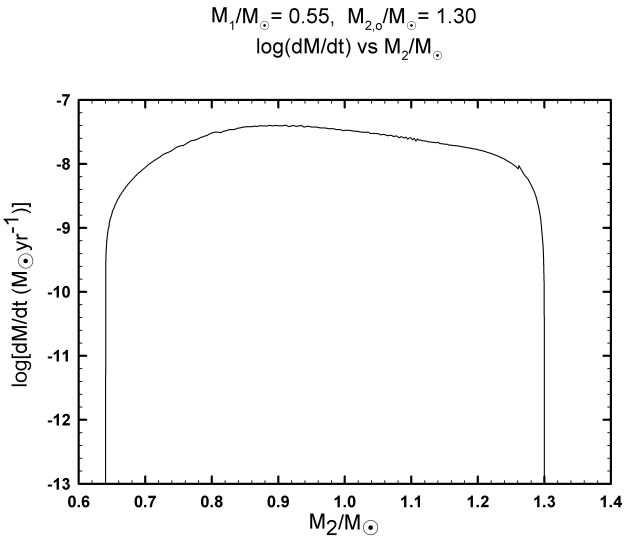

Figure 15: $\log\left[\frac{dM}{dt}\left(M_{\odot}yr^{-1}\right)\right]$ vs. Donor Mass $\left(\frac{M_2}{M_{\odot}}\right)$ - TTMT CV with starting masses $\left(\frac{M_1}{M_{\odot}}\right) = 0.55$ and $\left(\frac{M_2}{M_{\odot}}\right) = 1.30$

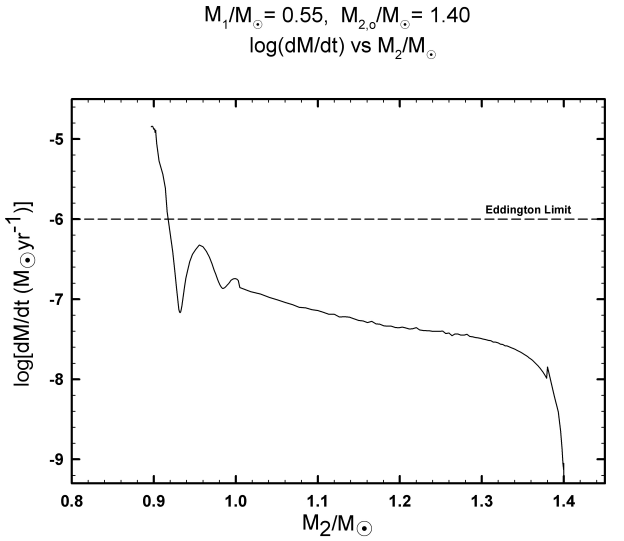

Figure 16: $\log\left[\frac{dM}{dt}\left(M_{\odot}yr^{-1}\right)\right]$ vs. Donor Mass $\left(\frac{M_2}{M_{\odot}}\right)$ - Latent Dynamically Unstable CV with starting masses $\left(\frac{M_1}{M_{\odot}}\right) = 0.55$ and $\left(\frac{M_2}{M_{\odot}}\right) = 1.40$

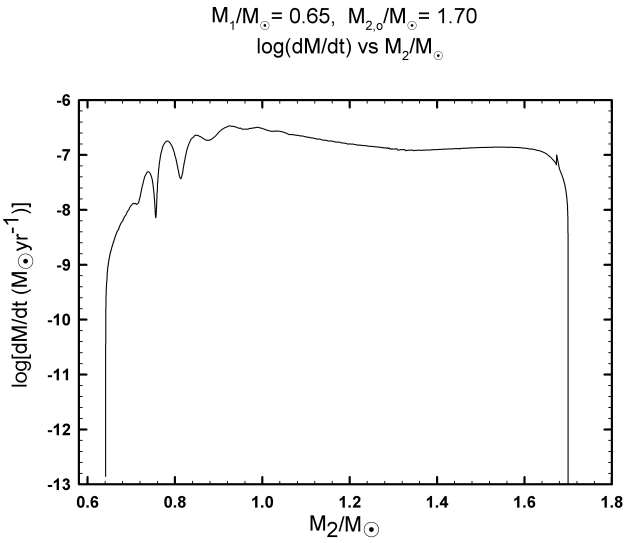

Figure 17: $\log\left[\frac{dM}{dt}\left(M_{\odot}yr^{-1}\right)\right]$ vs. Donor Mass $\left(\frac{M_2}{M_{\odot}}\right)$ - TTMT CV with starting masses $\left(\frac{M_1}{M_{\odot}}\right) = 0.65$ and $\left(\frac{M_2}{M_{\odot}}\right) = 1.70$

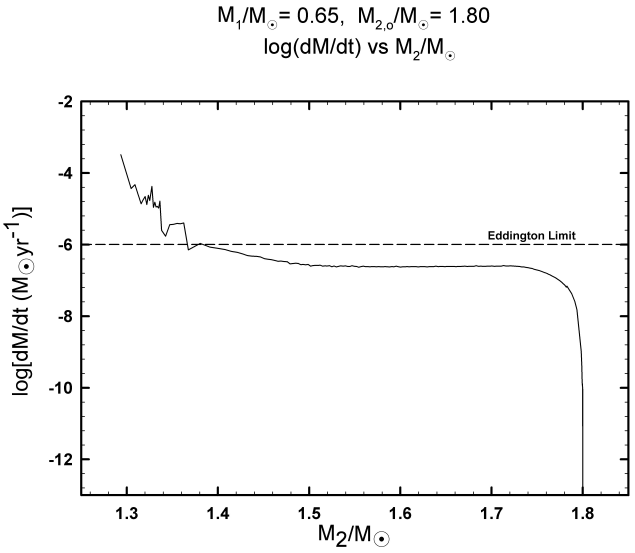

Figure 18: $\log\left[\frac{dM}{dt}\left(M_{\odot}yr^{-1}\right)\right]$ vs. Donor Mass $\left(\frac{M_2}{M_{\odot}}\right)$ - Latent Dynamically Unstable CV with starting masses $\left(\frac{M_1}{M_{\odot}}\right) = 0.65$ and $\left(\frac{M_2}{M_{\odot}}\right) = 1.80$

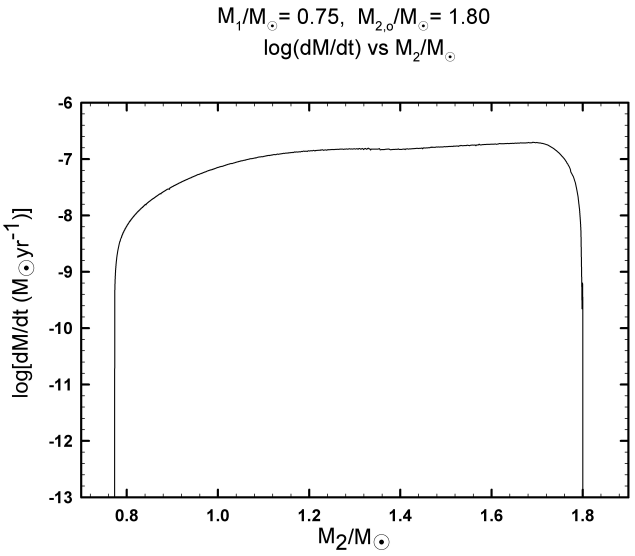

Figure 19: $\log\left[\frac{dM}{dt}\,(M_{\odot}yr^{-1})\right]$ vs. Donor Mass $\left(\frac{M_2}{M_{\odot}}\right)$ - TTMT CV with starting masses $\left(\frac{M_1}{M_{\odot}}\right) = 0.75$ and $\left(\frac{M_2}{M_{\odot}}\right) = 1.80$

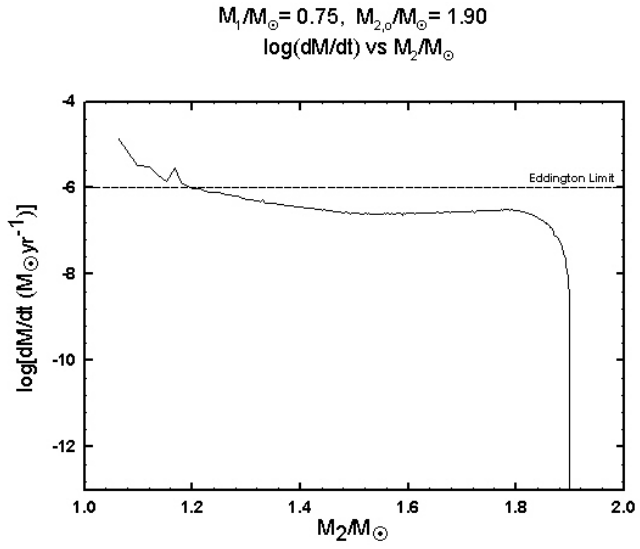

Figure 20: $\log\left[\frac{dM}{dt}\,(M_{\odot}yr^{-1})\right]$ vs. Donor Mass $\left(\frac{M_2}{M_{\odot}}\right)$ - TTMT CV with starting masses $\left(\frac{M_1}{M_{\odot}}\right) = 0.75$ and $\left(\frac{M_2}{M_{\odot}}\right) = 1.90$

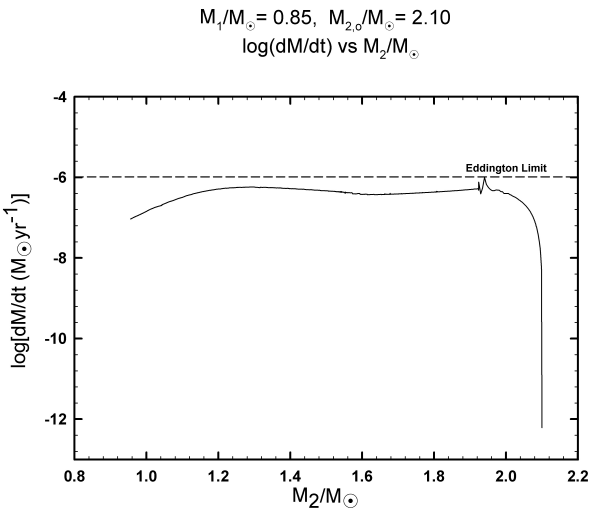

Figure 21: $\log\left[\frac{dM}{dt}\left(M_{\odot}yr^{-1}\right)\right]$vs. Donor Mass $\left(\frac{M_2}{M_{\odot}}\right)$ - TTMT CV with starting masses $\left(\frac{M_1}{M_{\odot}}\right) = 0.85$ and $\left(\frac{M_2}{M_{\odot}}\right) = 2.10$

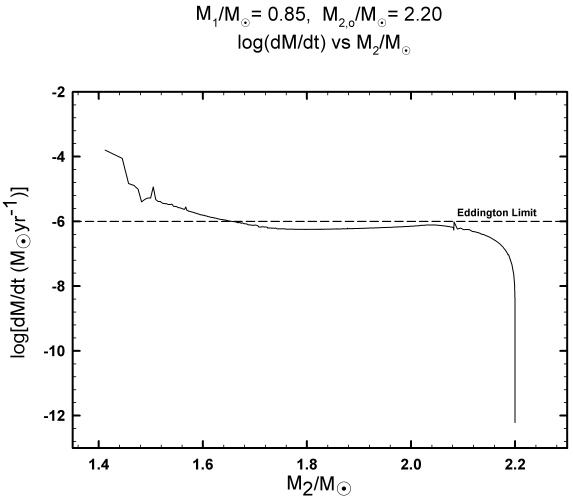

Figure 22: $\log\left[\frac{dM}{dt}\left(M_{\odot}yr^{-1}\right)\right]$vs. Donor Mass $\left(\frac{M_2}{M_{\odot}}\right)$ - Latent Dynamically Unstable CV with starting masses $\left(\frac{M_1}{M_{\odot}}\right) = 0.85$ and $\left(\frac{M_2}{M_{\odot}}\right) = 2.2$

3.4.2 Regression Line

Figure 23 shows the data with a curve that separates the plot into the two major regions of stability.

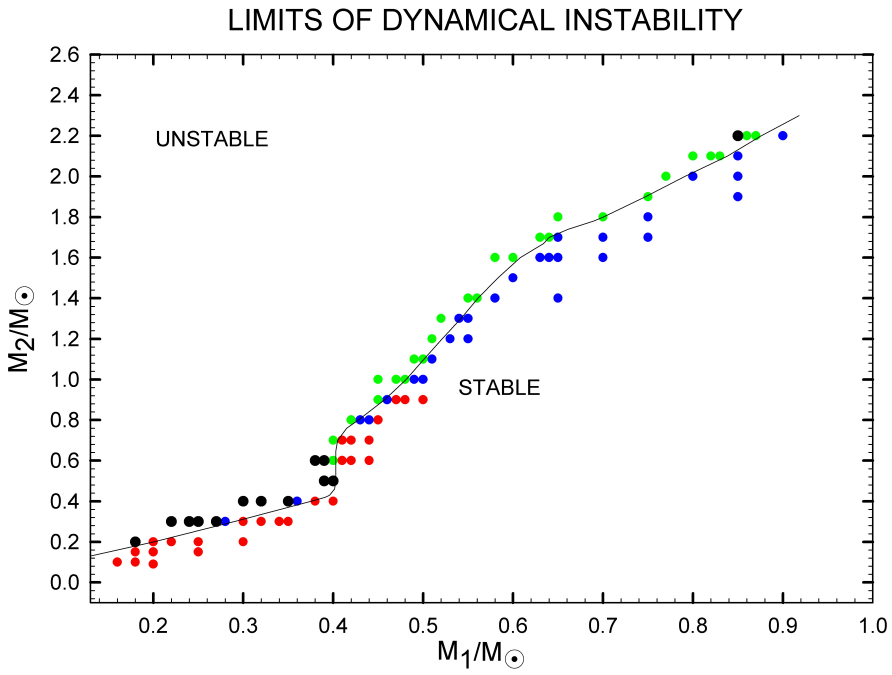

Figure 23: $\left(\frac{M_2}{M_\odot}\right)$ vs. $\left(\frac{M_1}{M_\odot}\right)$ - Line of Best Fit, with Data Displayed

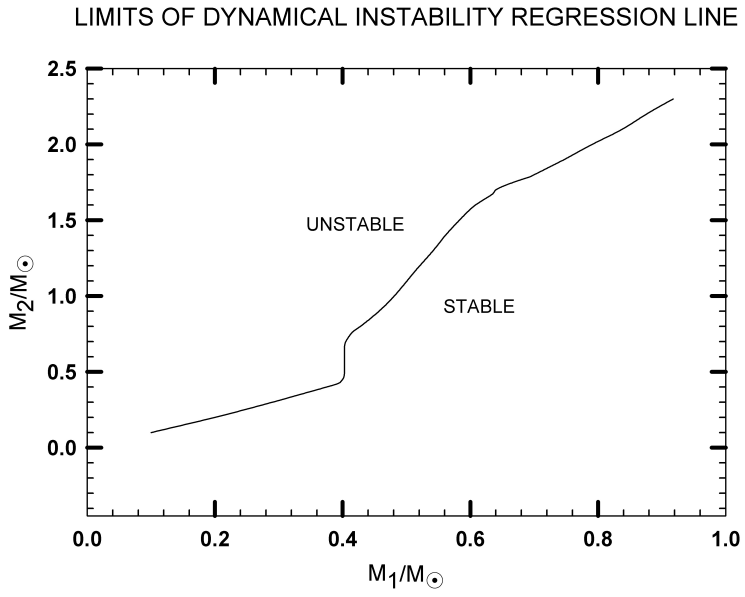

Figure 24: $\left(\frac{M_2}{M_\odot}\right)$ vs. $\left(\frac{M_1}{M_\odot}\right)$ - Line of Best Fit, without Data Displayed

It can be clearly seen from Figure 24 that this curve could be analyzed in separate parts. For our analysis, we will use two different approaches to obtain functional fits for this plot. The first method (section 3.4.3) will be a set of three interconnecting linear regressions used to described Figure 24 in three parts and the second method (section 3.4.4) will use a linear regression for the lower half and a quadratic regression for the upper half. The lower and upper halves are distinguished by the point at which the stars are no longer considered fully convective (i.e., $M_2 \lesssim 0.35 M_\odot$).

We can also see an almost vertical jump in the stability boundary right around this area. This jump occurs in an extremely small range of WD masses ($0.40 M_\odot \lesssim M_1 \lesssim 0.41 M_\odot$). Figures 25-30 clearly show the conditions needed to create a vertical jump like that. Figures 25-28 are presented in pairs with a fixed donor mass, $\left(\frac{M_2}{M_\odot}\right)$, while the WD mass $\left(\frac{M_1}{M_\odot}\right)$ is incremented one interval. This pairing clearly shows that the stability boundary is constrained between two fixed WD masses for a certain set of donor masses. Figure 29 constrains the beginning of the vertical jump, while Figure 30 is the upper bound of this vertical jump.

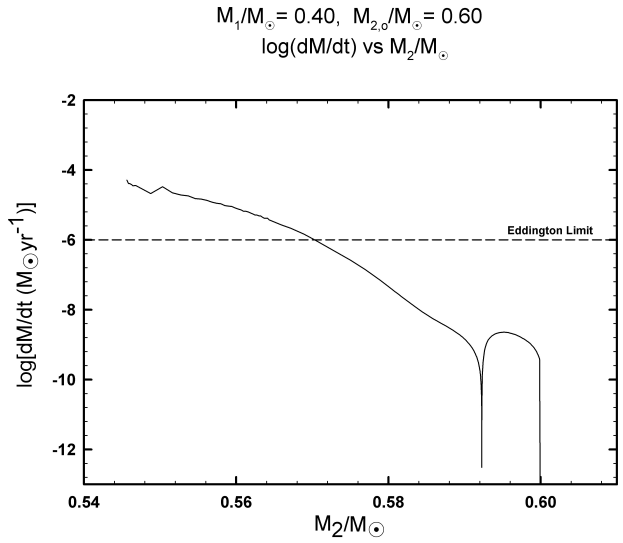

Figure 25: $\log\left[\frac{dM}{dt}\left(M_{\odot}yr^{-1}\right)\right]$vs. Donor Mass $\left(\frac{M_2}{M_{\odot}}\right)$ - Dynamically unstable CV with starting masses $\left(\frac{M_1}{M_{\odot}}\right) = 0.40$ and $\left(\frac{M_2}{M_{\odot}}\right) = 0.60$

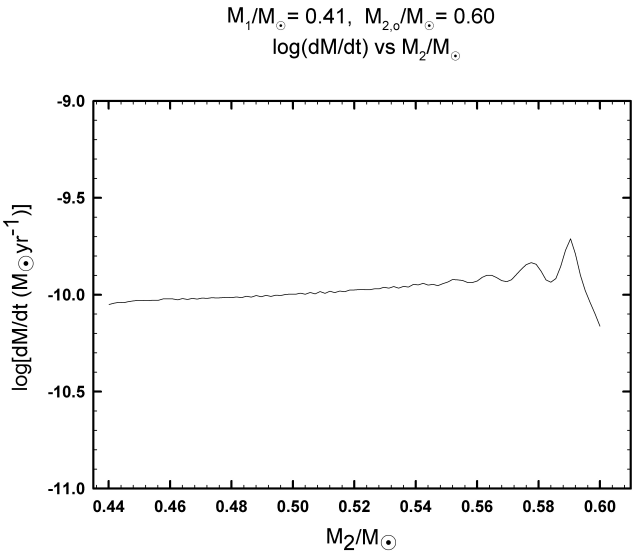

Figure 26: $\log\left[\frac{dM}{dt}\left(M_{\odot}yr^{-1}\right)\right]$vs. Donor Mass $\left(\frac{M_2}{M_{\odot}}\right)$ - Stable CV with starting masses $\left(\frac{M_1}{M_{\odot}}\right) = 0.41$ and $\left(\frac{M_2}{M_{\odot}}\right) = 0.60$

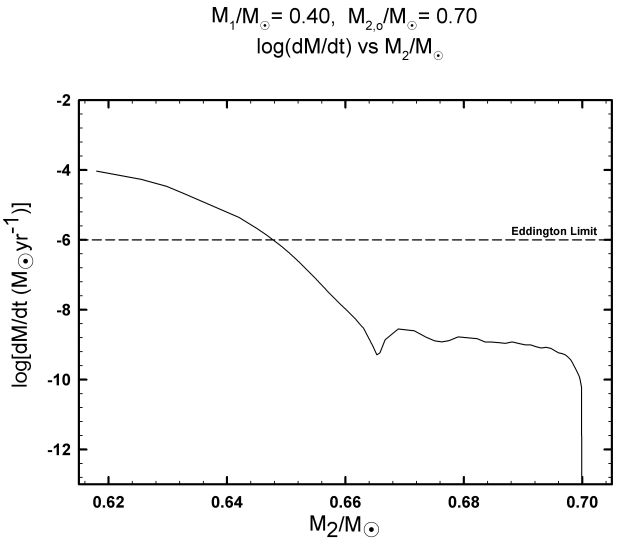

Figure 27: $\log\left[\frac{dM}{dt}\left(M_{\odot}yr^{-1}\right)\right]$vs. Donor Mass $\left(\frac{M_2}{M_{\odot}}\right)$ - Latent Dynamically unstable CV with starting masses $\left(\frac{M_1}{M_{\odot}}\right) = 0.40$ and $\left(\frac{M_2}{M_{\odot}}\right) = 0.70$

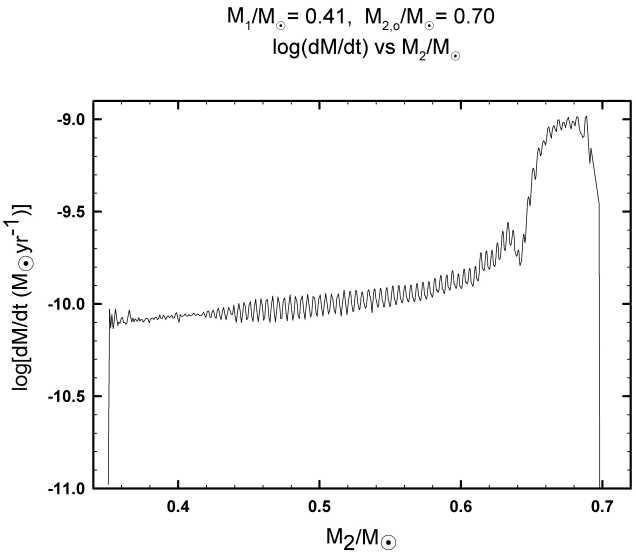

Figure 28: $\log\left[\frac{dM}{dt}\left(M_{\odot}yr^{-1}\right)\right]$vs. Donor Mass $\left(\frac{M_2}{M_{\odot}}\right)$ - Stable CV with starting masses $\left(\frac{M_1}{M_{\odot}}\right) = 0.41$ and $\left(\frac{M_2}{M_{\odot}}\right) = 0.70$

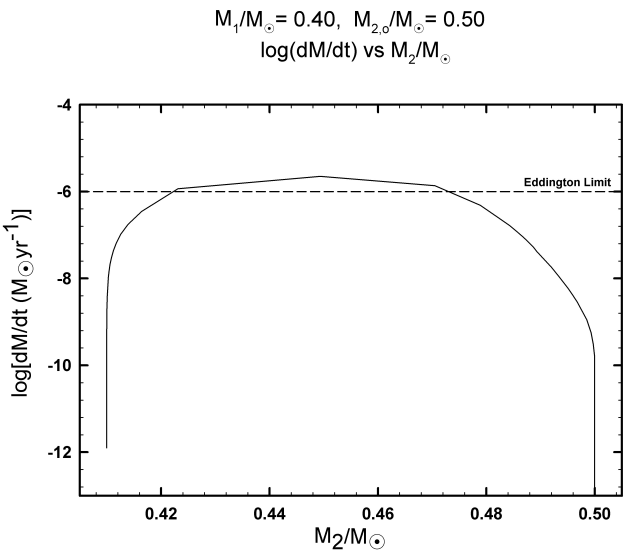

Figure 29: $\log\left[\frac{dM}{dt}\left(M_{\odot}yr^{-1}\right)\right]$vs. Donor Mass $\left(\frac{M_2}{M_{\odot}}\right)$ - Latent Dynamically unstable CV with starting masses $\left(\frac{M_1}{M_{\odot}}\right) = 0.40$ and $\left(\frac{M_2}{M_{\odot}}\right) = 0.50$

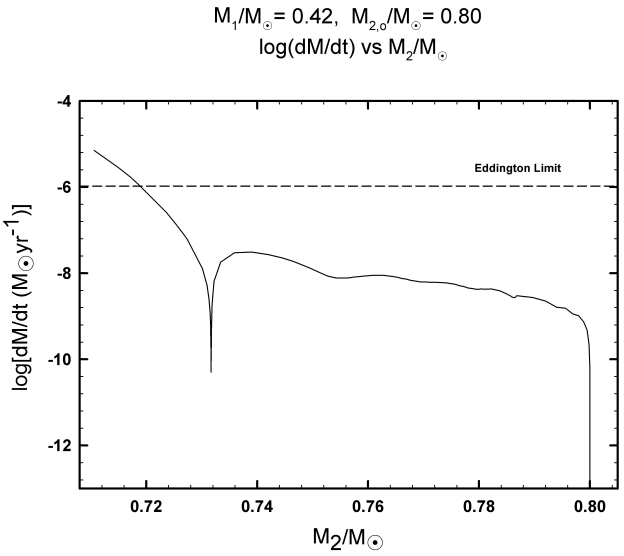

Figure 30: $\log\left[\frac{dM}{dt}\left(M_{\odot}yr^{-1}\right)\right]$vs. Donor Mass $\left(\frac{M_2}{M_{\odot}}\right)$ - Stable CV with starting masses $\left(\frac{M_1}{M_{\odot}}\right) = 0.42$ and $\left(\frac{M_2}{M_{\odot}}\right) = 0.80$

3.4.3 Three Part Linear Regression

For this analysis method the curve is divided into three linear sections that will be used to interpolate the curve separating the stable and unstable points. The three regions being used are as follows, $0.16M_{\odot} \lesssim M_1 < 0.40M_{\odot}$, $0.40M_{\odot} < M_1 \lesssim 0.62M_{\odot}$, and $0.62M_{\odot} \lesssim M_1 < 0.90M_{\odot}$ which we will refer to as the fully convective, convective envelope and radiative envelope regions respectively. The reason for this nomenclature is due to the fact that the structure of, the majority of the donor models is accurately described by these names. For example, the fully convective region is associated with convective stars having an $M_2 \lesssim 0.35M_{\odot}$, the convective envelope region roughly corresponds to models that have an $M_2 \lesssim 1.30M_{\odot}$ and the radiative envelope region is limited to $M_2 \gtrsim 1.30M_{\odot}$. Figure 31 plots the three regression lines (dashed lines labeled Regression I, II and III), and we can see that the discontinuity discussed in section 3.4.2 is located at $M_1 \cong 0.40M_{\odot}$.

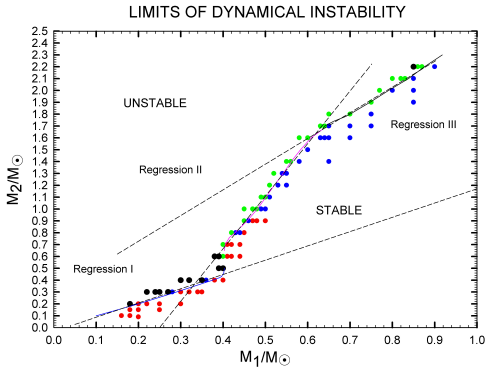

Figure 31: $\left(\frac{M_2}{M_{\odot}}\right)$ vs. $\left(\frac{M_1}{M_{\odot}}\right)$ - Using Three Linear Regressions to fit the Data

For the above linear regressions the slope can be defined as $a = \frac{\delta M_2}{\delta M_1}$, and b is the intercept. Therefore using Sigmaplot the slopes of each of the regressions can be calculated to result in a value ofyield an equation for q for each region.

For the fully convective region,

$$q_{cr} = 1.20 - \left(\frac{0.03}{M_1/M_{\odot}}\right) \tag{20}$$

Considering we used an idealized stellar index of $\xi = -1/3$ for our theoretical calculation (section 2.1.2), the numerical solution obtained through linear regression methods is in very good agreement. In fact, that is why a semi-analytic approach was taken in Chapter 2 - in order to justify some of the numerical results of this chapter.

Now for the convective envelope region we get,

$$q_{cr} = 4.43 - \left(\frac{1.11}{M_1/M_\odot}\right) \tag{21}$$

and for the radiative shell region

$$q_{cr} = 2.17 + \left(\frac{0.29}{M_1/M_\odot}\right). \tag{22}$$

The calculated R^2 values for these solutions are $R^2 = 0.9728$, $R^2 = 0.9965$, and $R^2 = 0.9969$ for the fully convective, convective envelope, and radiative envelope regions, respectively.

3.4.4 Linear and Quadratic Regression Combination

For this analysis method the curve is divided into two sections that will be used to interpolate the curve between the stable and unstable points. The first section of this calculation will use the same linear regression used in section 3.4.3 for the fully convective star region. The difference with this method is the attempt to merge the last two sections of the three part linear integration method into one quadratic regression line. The graphical results are shown in Figure 32.

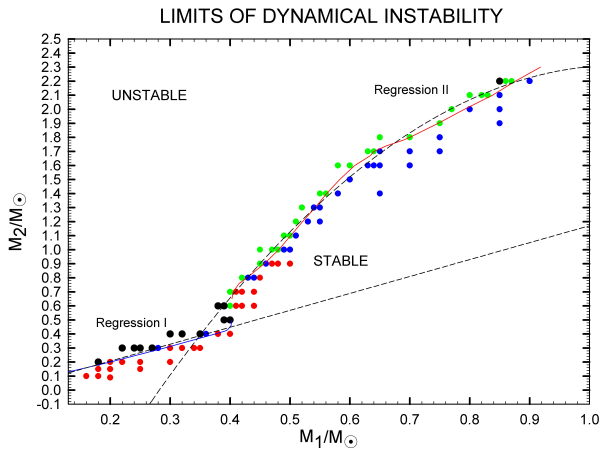

Figure 32: $\left(\frac{M_2}{M_\odot}\right)$ vs. $\left(\frac{M_1}{M_\odot}\right)$ - Using Linear and Quadratic Regressions to fit the Data

Therefore the fitted linear curve results in $q_{cr} = 1.20 - \left(\frac{3.91}{M_1/M_\odot}\right)$ (as before) and the quadratic curve yields

$$\frac{M_2}{M_\odot} = -3.9114\left(\frac{M_1}{M_\odot}\right)^2 + 8.2224\left(\frac{M_1}{M_\odot}\right) - 2.0069 \tag{23}$$

Then if we were to divide both sides by $\frac{M_1}{M_\odot}$, we would get,

$$q_{cr} = 8.2224 - \frac{2.0069 M_\odot}{M_1} - 3.9114\left(\frac{M_1}{M_\odot}\right) \tag{24}$$

with an $R^2 = 0.9952$. Note that the details of the regression analysis can be found in Appendix A.2.

4 Conclusions

From the analysis of the CV tracks it is evident that the structure of the donor star plays a key role in determining the limiting mass ratio. There is a large difference in q values from fully convective donors (equation (20)), to ones that just has a convective envelope (equation (21)) or even a radiative envelope (equation (22)). There are also no LDIs within the fully convective region. They seem to die out for any $M_2 \lesssim 0.6 M_\odot$. The most likely explanation for this behavior is the fact that the star is already fully convective, and therefore its thermal profile doesn't change drastically when mass is lost. Also the TTMT cases become narrow in range as M_2 decreases. Unlike the cases for LDIs, we do not believe that TTMT stops completely. If we were able to create an extremely fine grid, we believe that it would be possible to create tracks that result in TTMT, but that we would be unable to reproduce tracks that result in LDI for $M_2 \lesssim 0.35 M_\odot$.

In summary, we have explored the boundary separating stable and unstable mass transfer. We showed, using a semi-analytic approach, that instability is expected for the appropriate combination of high q values and low values of ξ. For the convective donor star case ($M \lesssim 0.35 \mathrm{M}_\odot$), we showed that the boundary occurs for $q_{cr} \cong 1$. Our numerical results are in good agreement with this estimation. The exact conditions enforcing dynamical instabilities are complicated and require numerical calculations of stellar structure and evolution. Finally, we have delineated the regions of initial condition space where it is possible to find CVs evolving as SSXSs (i.e., the putative progenitors of Type Ia Supernovae). We have also shown the conditions for which a merger (and destruction of the binary) should occur. The unexpected occurrence of very long-lived phases of rapid mass transfer (i.e., LDIs) shows that many more SSXSs may be able to undergo a Type Ia Supernova explosion than had been previously thought. This supposition needs further investigation.

4.1 Future Work

In this thesis we only investigated a donor star that was at one specific stage in its evolution (ZAMS) at the onset of mass transfer. This corresponds by far to the majority of observed CVs (Goliasch 2009 [17]).The results presented in this thesis do not allow us to determine how a CV's stability will be affected if mass transfer starts at a different evolutionary state. Further work should

include a study of different starting chemical compositions for the donor star to see how this would affect the stability conditions. Another aspect that requires further investigation is finding the exact solution of the Eddington limit on a case by case basis. The Eddington limit is non-constant and therefore should be investigated self-consistently for each model. The other possible avenue of exploration is to consider the possibility of some retention of mass. The means that not all of the mass would be lost through classical nova bursts. It would be interesting to investigate the effects this would have on the stability of the system (we note however that an analytic investigation was attempted by Soberman et al. 1997 [4]). However, we believe that based on the semi-analytic analysis presented in Chapter 2, the effects on stability would not be as large as those associated with different chemical and thermal profiles. This must be determined numerically.

A Sigmaplot Regression Results

A.1 Three Part Linear Regression Results

A.1.1 Linear Fit (Regression I)

Nonlinear Regression

[Variables]
x = col(14)
y = col(15)

reciprocal_y = 1/abs(y)
reciprocal_ysquare = 1/y^2

'Automatic Initial Parameter Estimate Functions
F(q)=ape(x,y,1,0,1)

[Parameters]
y0 = F(0)[1] "Auto {{previous: -0.0337455}}
a = F(0)[2] "Auto {{previous: 1.20476}}

[Equation]
f=y0+a*x
fit f to y
"fit f to y with weight reciprocal_y
"fit f to y with weight reciprocal_ysquare

[Constraints]
[Options]
tolerance=0.000100
stepsize=100
iterations=100

R = 0.98628358 Rsqr = 0.97275531 Adj Rsqr = 0.96821452

Standard Error of Estimate = 0.0248

	Coefficient	Std. Error	t	P
y0	-0.0337	0.0277	-1.2169	0.2693
a	1.2048	0.0823	14.6365	<0.0001

Table 1: Analysis of Variance

DF	SS	MS	F	P
Regression 1	0.1322	0.1322	214.2264	<0.0001

Residual 6 0.0037 0.0006
Total 7 0.1359 0.0194

PRESS = 0.0069
Durbin-Watson Statistic = 0.6800
Normality Test: K-S Statistic = 0.2480
Significance Level = 0.6426
Constant Variance Test: Passed (P = 0.2604)
Power of performed test with alpha = 0.0500: 0.9998

Table 2: Regression Diagnostics

Row	Predicted	Residual	Std. Res.	Stud. Res.	Stud. Del. Res.
1	0.0867	0.0133	0.5342	0.9086	0.8932
2	0.2072	-0.0072	-0.2901	-0.3424	-0.3156
3	0.3156	-0.0156	-0.6294	-0.6766	-0.6426
4	0.4180	-0.0180	-0.7262	-0.7918	-0.7638
5	0.4373	-0.0173	-0.6971	-0.7703	-0.7407
6	0.4433	-0.0133	-0.5370	-0.5963	-0.5613
7	0.4500	0.0100	0.4040	0.4513	0.4192
8	0.4518	0.0482	1.9415	2.1727	4.2948

Table 3: Influence Diagnostics

Row	Cook's Dist	Leverage	DFFITS
1	0.7814	0.6543	1.2289
2	0.0230	0.2820	-0.1978
3	0.0356	0.1346	-0.2534
4	0.0591	0.1587	-0.3318
5	0.0656	0.1810	-0.3483
6	0.0415	0.1892	-0.2711
7	0.0253	0.1987	0.2087
8	0.5954	0.2014	2.1571

Table 4: 95% Confidence

Row	Predicted	Regr. 5%	Regr. 95%	Pop. 5%	Pop. 95%
1	0.0867	0.0376	0.1359	0.0086	0.1649
2	0.2072	0.1749	0.2395	0.1384	0.2760
3	0.3156	0.2933	0.3379	0.2509	0.3804
4	0.4180	0.3938	0.4423	0.3526	0.4835
5	0.4373	0.4115	0.4632	0.3713	0.5034
6	0.4433	0.4169	0.4698	0.3771	0.5096
7	0.4500	0.4229	0.4771	0.3834	0.5165
8	0.4518	0.4245	0.4791	0.3851	0.5184

A.1.2 Linear Fit (Regression II)

Nonlinear Regression

[Variables]
x = col(16)
y = col(17)

reciprocal_y = 1/abs(y)
reciprocal_ysquare = 1/y^2

'Automatic Initial Parameter Estimate Functions
F(q)=ape(x,y,1,0,1)

[Parameters]
y0 = F(0)[1] "Auto {{previous: -1.1087}}
a = F(0)[2] "Auto {{previous: 4.43387}}

[Equation]
f=y0+a*x
fit f to y
"fit f to y with weight reciprocal_y
"fit f to y with weight reciprocal_ysquare

[Constraints]
[Options]
tolerance=0.000100
stepsize=100
iterations=100

R = 0.99824568 Rsqr = 0.99649444 Adj Rsqr = 0.99617575

Standard Error of Estimate = 0.0218

	Coefficient	Std. Error	t	P
y0	-1.1087	0.0403	-27.4851	<0.0001
a	4.4339	0.0793	55.9184	<0.0001

Table 5: Analysis of Variance

DF	SS	MS	F	P
Regression 1	1.4818	1.4818	3126.8711	<0.0001

Residual 11 0.0052 0.0005
Total 12 1.4870 0.1239

PRESS = 0.0081
Durbin-Watson Statistic = 1.1189
Normality Test: K-S Statistic = 0.1627 Significance Level = 0.8490
Constant Variance Test: Passed (P = 0.8632)
Power of performed test with alpha = 0.0500: 1.0000

Table 6: Regression Diagnostics

Row	Predicted	Residual	Std. Res.	Stud. Res.	Stud.Del. Res.
1	0.6782	-0.0282	-1.2932	-1.4546	-1.5432
2	0.6870	0.0130	0.5963	0.6685	0.6508
3	0.7314	0.0286	1.3158	1.4527	1.5408
4	0.7890	0.0110	0.5054	0.5487	0.5305
5	0.9176	-0.0176	-0.8076	-0.8536	-0.8423
6	1.0240	-0.0240	-1.1022	-1.1512	-1.1704
7	1.1127	-0.0127	-0.5821	-0.6058	-0.5875
8	1.2013	-0.0013	-0.0619	-0.0646	-0.0616
9	1.2945	0.0055	0.2545	0.2678	0.2562
10	1.3787	0.0213	0.9783	1.0438	1.0485
11	1.4762	0.0238	1.0911	1.1918	1.2176
12	1.5871	0.0129	0.5928	0.6726	0.6549
13	1.7024	-0.0324	-1.4873	-1.7835	-2.0170

Table 7: Influence Diagnostics

Row	Cook's Dist	Leverage	DFFITS
1	0.2805	0.2096	-0.7947
2	0.0574	0.2043	0.3298
3	0.2311	0.1797	0.7211
4	0.0269	0.1516	0.2242
5	0.0427	0.1050	-0.2885
6	0.0602	0.0833	-0.3529
7	0.0153	0.0770	-0.1697
8	0.0002	0.0812	-0.0183
9	0.0039	0.0971	0.0840
10	0.0754	0.1216	0.3900
11	0.1371	0.1618	0.5350
12	0.0650	0.2232	0.3511
13	0.6967	0.3046	-1.3349

Table 8: 95% Confidence

Row	Predicted	Regr. 5%	Regr. 95%	Pop. 5%	Pop. 95%
1	0.6782	0.6562	0.7001	0.6255	0.7308
2	0.6870	0.6654	0.7087	0.6344	0.7396
3	0.7314	0.7110	0.7517	0.6793	0.7834
4	0.7890	0.7703	0.8077	0.7376	0.8404
5	0.9176	0.9021	0.9331	0.8672	0.9679
6	1.0240	1.0102	1.0378	0.9741	1.0739
7	1.1127	1.0994	1.1260	1.0629	1.1624
8	1.2013	1.1877	1.2150	1.1515	1.2512
9	1.2945	1.2795	1.3094	1.2443	1.3446
10	1.3787	1.3620	1.3954	1.3280	1.4294
11	1.4762	1.4570	1.4955	1.4246	1.5279
12	1.5871	1.5645	1.6097	1.5341	1.6401
13	1.7024	1.6759	1.7288	1.6477	1.7571

A.1.3 Linear Fit (Regression III)

Nonlinear Regression

[Variables]
x = col(18)
y = col(19)

reciprocal_y = 1/abs(y)

reciprocal_ysquare = 1/y^2

'Automatic Initial Parameter Estimate Functions
F(q)=ape(x,y,1,0,1)

[Parameters]
y0 = F(0)[1] "Auto {{previous: 0.294825}}
a = F(0)[2] "Auto {{previous: 2.1673}}

[Equation]
f=y0+a*x
fit f to y
"fit f to y with weight reciprocal_y
"fit f to y with weight reciprocal_ysquare

[Constraints]
[Options]
tolerance=0.000100
stepsize=100
iterations=100

R = 0.99843013 Rsqr = 0.99686272 Adj Rsqr = 0.99647057

Standard Error of Estimate = 0.0131

	Coefficient	Std. Error	t	P
y0	0.2948	0.0325	9.0770	<0.0001
a	2.1673	0.0430	50.4181	<0.0001

Table 9: Analysis of Variance

DF	SS	MS	F	P
Regression 1	0.4379	0.4379	2541.9835	<0.0001

Residual 8 0.0014 0.0002

Total 9 0.4393 0.0488

PRESS = 0.0024
Durbin-Watson Statistic = 0.8577

Normality Test: K-S Statistic = 0.2435 Significance Level = 0.5317
Constant Variance Test: Passed (P = 0.8379)
Power of performed test with alpha = 0.0500: 1.0000

Table 10: Regression Diagnostics

Row	Predicted	Residual	Std. Res.	Stud. Res.	Stud. Del. Res.
1	1.6689	0.0011	0.0843	0.0969	0.0907
2	1.6819	0.0181	1.3792	1.5701	1.7658
3	1.7274	0.0126	0.9592	1.0617	1.0715
4	1.7881	-0.0081	-0.6168	-0.6647	-0.6397
5	1.8119	-0.0119	-0.9093	-0.9728	-0.9691
6	1.9138	-0.0138	-1.0513	-1.1082	-1.1267
7	2.0092	-0.0092	-0.6979	-0.7433	-0.7206
8	2.1110	-0.0110	-0.8398	-0.9298	-0.9209
9	2.1934	0.0066	0.5043	0.5911	0.5654
10	2.2844	0.0156	1.1880	1.5400	1.7175

Table 11: Influence Diagnostics

Row	Cook's Dist	Leverage	DFFITS
1	0.0015	0.2428	0.0514
2	0.3648	0.2284	0.9606
3	0.1269	0.1838	0.5085
4	0.0357	0.1391	-0.2572
5	0.0683	0.1262	-0.3682
6	0.0683	0.1001	-0.3757
7	0.0372	0.1186	-0.2643
8	0.0976	0.1842	-0.4376
9	0.0652	0.2719	0.3455
10	0.8069	0.4049	1.4167

Table 12: 95% Confidence

Row	Predicted	Regr. 5%	Regr. 95%	Pop. 5%	Pop. 95%
1	1.6689	1.6540	1.6838	1.6352	1.7026
2	1.6819	1.6674	1.6964	1.6484	1.7154
3	1.7274	1.7144	1.7404	1.6945	1.7603
4	1.7881	1.7768	1.7994	1.7558	1.8204
5	1.8119	1.8012	1.8227	1.7798	1.8441
6	1.9138	1.9042	1.9234	1.8821	1.9455
7	2.0092	1.9987	2.0196	1.9771	2.0412
8	2.1110	2.0980	2.1240	2.0781	2.1440
9	2.1934	2.1776	2.2092	2.1592	2.2275
10	2.2844	2.2651	2.3037	2.2485	2.3203

A.2 Linear and Quadratic Method Results

A.2.1 Linear Fit (Regression I)

Nonlinear Regression

[Variables]
x = col(14)
y = col(15)

reciprocal_y = 1/abs(y)
reciprocal_ysquare = 1/y^2

'Automatic Initial Parameter Estimate Functions
F(q)=ape(x,y,1,0,1)

[Parameters]
y0 = F(0)[1] "Auto {{previous: -0.0337455}}
a = F(0)[2] "Auto {{previous: 1.20476}}

[Equation]
f=y0+a*x
fit f to y
"fit f to y with weight reciprocal_y
"fit f to y with weight reciprocal_ysquare

[Constraints]
[Options]

tolerance=0.000100
stepsize=100
iterations=100

R = 0.98628358 Rsqr = 0.97275531 Adj Rsqr = 0.96821452

Standard Error of Estimate = 0.0248

	Coefficient	Std. Error	t	P
y0	-0.0337	0.0277	-1.2169	0.2693
a	1.2048	0.0823	14.6365	<0.0001

Table 13: Analysis of Variance

DF	SS	MS	F	P
Regression 1	0.1322	0.1322	214.2264	<0.0001

Residual 6 0.0037 0.0006
Total 7 0.1359 0.0194

PRESS = 0.0069
Durbin-Watson Statistic = 0.6800
Normality Test: K-S Statistic = 0.2480
Significance Level = 0.6426
Constant Variance Test: Passed (P = 0.2604)
Power of performed test with alpha = 0.0500: 0.9998

Table 14: Regression Diagnostics

Row	Predicted	Residual	Std. Res.	Stud. Res.	Stud. Del. Res.
1	0.0867	0.0133	0.5342	0.9086	0.8932
2	0.2072	-0.0072	-0.2901	-0.3424	-0.3156
3	0.3156	-0.0156	-0.6294	-0.6766	-0.6426
4	0.4180	-0.0180	-0.7262	-0.7918	-0.7638
5	0.4373	-0.0173	-0.6971	-0.7703	-0.7407
6	0.4433	-0.0133	-0.5370	-0.5963	-0.5613
7	0.4500	0.0100	0.4040	0.4513	0.4192
8	0.4518	0.0482	1.9415	2.1727	4.2948

Table 15: Influence Diagnostics

Row	Cook's Dist	Leverage	DFFITS
1	0.7814	0.6543	1.2289
2	0.0230	0.2820	-0.1978
3	0.0356	0.1346	-0.2534
4	0.0591	0.1587	-0.3318
5	0.0656	0.1810	-0.3483
6	0.0415	0.1892	-0.2711
7	0.0253	0.1987	0.2087
8	0.5954	0.2014	2.1571

Table 16: 95% Confidence

Row	Predicted	Regr. 5%	Regr. 95%	Pop. 5%	Pop. 95%
1	0.0867	0.0376	0.1359	0.0086	0.1649
2	0.2072	0.1749	0.2395	0.1384	0.2760
3	0.3156	0.2933	0.3379	0.2509	0.3804
4	0.4180	0.3938	0.4423	0.3526	0.4835
5	0.4373	0.4115	0.4632	0.3713	0.5034
6	0.4433	0.4169	0.4698	0.3771	0.5096
7	0.4500	0.4229	0.4771	0.3834	0.5165
8	0.4518	0.4245	0.4791	0.3851	0.5184

A.2.2 Quadratic Fit (Regression II)

Nonlinear Regression

[Variables]
x = col(16)
y = col(17)

reciprocal_y = 1/abs(y)
reciprocal_ysquare = 1/y^2

'Automatic Initial Parameter Estimate Functions
F(q)=ape(x,y,2,0,1)

[Parameters]

y0 = F(0)[1] "Auto {{previous: -2.00694}}
a = F(0)[2] "Auto {{previous: 8.22237}}
b = F(0)[3] "Auto {{previous: -3.91142}}

[Equation]
f=y0+a*x+b*x^2
fit f to y
"fit f to y with weight reciprocal_y
"fit f to y with weight reciprocal_ysquare

[Constraints]
[Options]
tolerance=0.000100
stepsize=100
iterations=100

R = 0.99760712 Rsqr = 0.99521997 Adj Rsqr = 0.99471681

Standard Error of Estimate = 0.0371

	Coefficient	Std. Error	t	P
y0	-2.0069	0.1366	-14.6920	<0.0001
a	8.2224	0.4433	18.5492	<0.0001
	-3.9114	0.3437	-11.3816	<0.0001

Table 17: Analysis of Variance

DF	SS	MS	F	P
Regression 2	5.4520	2.7260	1977.9372	<0.0001

Residual 19 0.0262 0.0014
Total 21 5.4782 0.2609
PRESS = 0.0399
Durbin-Watson Statistic = 0.5084
Normality Test: K-S Statistic = 0.1371 Significance Level = 0.7720
Constant Variance Test: Passed (P = 0.0507)
Power of performed test with alpha = 0.0500: 1.0000

Table 18: Regression Diagnostics

Row	Predicted	Residual	Std. Res.	Stud. Res.	Stud. Del. Res.
1	0.6714	-0.0214	-0.5772	-0.6524	-0.6422
2	0.6816	0.0184	0.4969	0.5592	0.5489
3	0.7317	0.0283	0.7622	0.8417	0.8349
4	0.7957	0.0043	0.1151	0.1246	0.1213
5	0.9338	-0.0338	-0.9102	-0.9585	-0.9564
6	1.0431	-0.0431	-1.1602	-1.2081	-1.2238
7	1.1307	-0.0307	-0.8270	-0.8576	-0.8514
8	1.2152	-0.0152	-0.4094	-0.4243	-0.4150
9	1.3006	-0.0006	-0.0149	-0.0155	-0.0151
10	1.3748	0.0252	0.6786	0.7065	0.6969
11	1.4573	0.0427	1.1514	1.2032	1.2184
12	1.5464	0.0536	1.4451	1.5161	1.5739
13	1.6338	0.0362	0.9744	1.0253	1.0267
14	1.6533	0.0467	1.2590	1.3253	1.3541
15	1.7191	0.0209	0.5638	0.5941	0.5837
16	1.8014	-0.0214	-0.5776	-0.6085	-0.5981
17	1.8321	-0.0321	-0.8654	-0.9113	-0.9070
18	1.9526	-0.0526	-1.4159	-1.4900	-1.5432
19	2.0497	-0.0497	-1.3376	-1.4182	-1.4597
20	2.1366	-0.0366	-0.9869	-1.0811	-1.0862
21	2.1943	0.0057	0.1528	0.1786	0.1740
22	2.2449	0.0551	1.4829	2.0388	2.2452

Table 19: Influence Diagnostics

Row	Cook's Dist	Leverage	DFFITS
1	0.0394	0.2172	-0.3383
2	0.0278	0.2105	0.2834
3	0.0518	0.1798	0.3910
4	0.0009	0.1471	0.0504
5	0.0334	0.0983	-0.3158
6	0.0410	0.0777	-0.3551
7	0.0185	0.0702	-0.2340
8	0.0045	0.0691	-0.1131
9	0.0000	0.0723	-0.0042
10	0.0140	0.0774	0.2019
11	0.0444	0.0843	0.3696
12	0.0771	0.0915	0.4993
13	0.0375	0.0968	0.3361
14	0.0633	0.0976	0.4453
15	0.0130	0.0993	0.1938
16	0.0136	0.0989	-0.1982
17	0.0302	0.0983	-0.2995
18	0.0794	0.0969	-0.5055
19	0.0832	0.1104	-0.5143
20	0.0780	0.1667	-0.4859
21	0.0039	0.2685	0.1054
22	1.2337	0.4710	2.1185

Table 20: 95% Confidence

Row	Predicted	Regr. 5%	Regr. 95%	Pop. 5%	Pop. 95%
1	0.6714	0.6352	0.7076	0.5857	0.7572
2	0.6816	0.6459	0.7172	0.5961	0.7670
3	0.7317	0.6988	0.7647	0.6473	0.8161
4	0.7957	0.7659	0.8255	0.7125	0.8789
5	0.9338	0.9094	0.9582	0.8524	1.0152
6	1.0431	1.0214	1.0647	0.9624	1.1237
7	1.1307	1.1101	1.1513	1.0503	1.2111
8	1.2152	1.1948	1.2356	1.1349	1.2955
9	1.3006	1.2797	1.3214	1.2201	1.3810
10	1.3748	1.3532	1.3964	1.2942	1.4555
11	1.4573	1.4347	1.4798	1.3763	1.5382
12	1.5464	1.5229	1.5699	1.4652	1.6275
13	1.6338	1.6097	1.6580	1.5525	1.7152
14	1.6533	1.6290	1.6775	1.5719	1.7347
15	1.7191	1.6946	1.7436	1.6376	1.8005
16	1.8014	1.7770	1.8259	1.7200	1.8829
17	1.8321	1.8078	1.8565	1.7507	1.9136
18	1.9526	1.9284	1.9768	1.8712	2.0339
19	2.0497	2.0238	2.0755	1.9678	2.1315
20	2.1366	2.1049	2.1684	2.0527	2.2206
21	2.1943	2.1541	2.2346	2.1068	2.2818
22	2.2449	2.1916	2.2983	2.1507	2.3392

References

[1] Dubeau, E. P. (2009), "Radio Ejection and the Orbital Period Gap in the Distribution of Binary Millisecond Pulsars", MSc Thesis (Bishop's University)

[2] "Rappaport, S., Verbunt, F., and Joss, P.C. (1983), "A New Technique for Calculations of Binary Stellar Evolution, With Application to Magnetic Braking", Astrophys. J. **275**, 713

[3] Eggleton, P. P. (1983), "Approximations to the Radii of Roche lobes", Astrophys. J. **268**, 368

[4] Soberman, G. E., Phinney, E. S., van den Heuvel, E. P. J. (1997), "Stability Criteria for Mass Transfer in Binary Stellar Evolution", Astron. Astrophys. **327**, 620

[5] Hjellming, M. S., Webbink, R. F. (1987), "Thresholds for Rapid Mass Transfer in Binary Systems. I - Polytropic Models"

[6] Rappaport, S., Pfahl, E., Rasio, F. A., Podsiadlowski, P. (2001), "Evolution of Binary and Multiple Star Systems", ASP Conference Series **229**, 409

[7] King, A.R., Kolb, U. (1999), "The Evolution of Black Hole Mass and Angular Momentum", MNRAS **305**, 654

[8] Soria, R. (2003), "X-ray Properties of Spiral Galaxies", IAU Symp. **214**, 59S

[9] Rappaport, S., Joss, P. C. (1982), "The Evolution of Highly Compact Binary Stellar Systems", Astrophys. J. **254**, 616

[10] Han, Z., Podsiadlowski, P., Tout, C. A. (2002), "Criterion for Dynamical Instability of Mass Transfer in Binary Evolution", ASP Conference Series **279**, 297

[11] Tout, C. A., Aarseth, S. J., Pols, O. R., Eggleton, P. P. (1997), "Rapid binary star evolution for N-body simulations and population synthesis", MNRAS **291**, 732

[12] King, A. R., Schenker, K., Kolb, U., Davies, M. B. (2001), "The Minimum Orbital Period in Thermal Time-Scale mass Transfer", MNRAS **321**, 327

[13] Ivanova, N., Taam, R. E. (2004), "Thermal Timescale Mass Transfer and the Evolution of White Dwarf Binaries", Astrophys. J. **601**, 1058

[14] de Kool, M. (1992), "Statistics of Cataclysmic Variable formation", Astron. Astrophys. **261**, 188

[15] Hilditch, R.W. (2001), "An Introduction to Close Binary Stars" (Cambridge: Cambridge University Press)

[16] D'Souza, M. C. R., Molt, P. M., Tohline, J. E., Framk, J. (2005), "Numerical Simulations of the Onset and Stability of Dynamical Mass Transfer in Binaries", Astrophys. J. **643**, 381

[17] Goliasch, J. (2009), "Population Synthesis of Cataclysmic Variables", MSc Thesis (Bishop's University), to be submitted

[18] DiStefano, R., Nelson, L. A., Lee, W., Wood, T. H., and Rappaport, S. (1996), "Luminous Super Soft X-ray Sources as Type Ia Progenitors", Thermonuclear Supernovae, (Berlin: Springer Verlag), 147.